EES Solar

PAPER

View Article Online
View Journal

Cite this: DOI: 10.1039/d5el00216h

The complexity of classical Marcus analysis for charge transfer states in organic photovoltaics

Liming Liu,[a] Weitang Li,[a] Sha Liu,[b] Xinhui Lu[c] and Jun Yan*[a]

Received 26th December 2025
Accepted 31st March 2026

DOI: 10.1039/d5el00216h

rsc.li/EESSolar

Classical Marcus theory is widely used in organic photovoltaics (OPVs) to extract charge transfer (CT) state properties from electroluminescence (EL) and sensitive external quantum efficiency (s-EQE) spectra. However, practical donor–acceptor blends often exhibit complications such as overlap between CT and localized exciton (LE) emissions, large static energetic disorder, and weak CT oscillator strengths, all of which can limit the accuracy of simple Marcus analysis. This article discusses those issues in detail and provides a practical guide to Marcus-based CT analysis for complex cases with invisible CT states and large static disorder. An open-source Python package is released to enable semi-automated classical Marcus analysis when CT is clearly visible.

Broader context

The classical Marcus theory serves as a standard framework for experimentally determining the properties of charge transfer states in organic photovoltaics. Although it has been highly successful for traditional systems with large energy offsets, it encounters significant limitations when applied to state-of-the-art non-fullerene acceptor-based systems. Here, we provide a detailed critique of potential issues and errors arising from the application of classical Marcus analysis. We also propose practical guidelines for more accurately estimating charge transfer state properties in complex systems—such as those exhibiting large static disorder or spectral overlap among excited states. Furthermore, this work introduces a computational toolkit to facilitate reliable classical Marcus analysis when charge transfer states are spectroscopically resolvable.

1 Introduction

Electron transfer is a fundamental process in chemistry, physics and biology, underpinning phenomena ranging from photosynthesis to energy conversion devices.[1–7] A modern quantitative description of this process began with the pioneering work of Rudolph Arthur Marcus in the mid-1950s. In 1956, Marcus proposed a theoretical framework in a series of papers,[8–14] which provided a quantitative description of the electron transfer reaction rate for the first time, known as Marcus theory. This theory is applicable to the reaction systems without chemical bond formation or cleavage, and the free energy of the system is expressed as a function of the collective nuclear coordinates, which replaces the application of Eyring's transition state theory in this kind of reaction.[10]

In the classical Marcus theory, the initial state (donor–acceptor pair, D–A) and the final state (ion pair, D^{-}–A^{+}) are represented by two intersecting parabolic potential energy surfaces, respectively.[15,16] The electron transfer rate depends on the energy barrier height at the intersection of these two curves.[17] This process involves two key parameters: one is the difference in Gibbs free energy ΔG^0 of the reaction, which reflects the thermodynamic driving force; the second is the reorganization energy λ, which represents the energy required to adjust the nuclear configuration of the reactant (including the surrounding solvent or medium) to the product state without electron transfer. This description follows from the Franck–Condon principle,[18,19] which states that electron transfer occurs on a time scale much faster than nuclear motion, *i.e.* the Born–Oppenheimer approximation.

One of the most striking and counterintuitive predictions of the Marcus model is the "inverted region" phenomenon.[9] The general chemical intuition is that the reaction rate increases with the increase in thermodynamic driving force. However, Marcus theory points out that for high driving force reactions (*i.e.*, $-\Delta G^0 > \lambda$), a further increase in the driving force will lead to a reduction in the rate. The experimental verification of the inverted region not only strongly supports the core hypothesis of the theory, but also provides an important basis for understanding the nonradiative transitions with large energy separation between initial and final states in organic optoelectronic devices.[20–23]

[a]Guangdong Basic Research Center of Excellence for Aggregate Science, School of Science and Engineering, The Chinese University of Hong Kong (Shenzhen), Longgang, Shenzhen, Guangdong, 518172, P.R. China. E-mail: yanjun@cuhk.edu.cn
[b]Dongguan Key Laboratory of Interdisciplinary Science for Advanced Materials and Large-Scale Scientific Facilities, School of Physical Sciences, Great Bay University, Dongguan, Guangdong, 523000, P. R. China
[c]Department of Physics, The Chinese University of Hong Kong, New Territories, Hong Kong SAR 999077, China

Marcus theory was originally established for outer electron transfer reactions in polar solvents. In this model, the reorganization of solvent continuum is the main source of the energy barrier. In organic semiconductors, the charge transfer environment includes both low-frequency lattice vibrations and high-frequency intramolecular vibrational modes. Since the vibrational energy of many molecules is higher than the thermal energy (k_BT) at room temperature, they must be treated using quantum mechanics.[24] This demand promoted the development of the semi-classical Marcus–Levich–Jortner (MLJ) theory,[2] in which electron transfer can occur not only through thermal activation, but also through the nuclear tunneling effect mediated by the overlap of vibrational wavefunctions. This extension makes the electron transfer theory more suitable for solid-state systems and is of key significance.[25–27]

In organic photovoltaics (OPVs), Marcus theory has gradually developed from a predictive framework of reaction rates to a key diagnostic tool. The performance of OPV devices largely depends on the open circuit voltage (V_{oc}), which is mainly limited by the energy loss in the process of photon-to-electricity conversion.[28,29] The core of this process lies at the donor–acceptor interface: upon photon absorption, excitons are generated and subsequently dissociate to form a charge transfer (CT) state at the interface.[30,31] Therefore, the CT state is the key intermediate state for charge generation and recombination,[32–34] and its energy (E_{CT}) is closely related to the thermodynamic limit for V_{oc} and needs to be accurately measured. Vandewal *et al.* pioneered the measurement of CT states *via* simultaneously fitting sensitive external quantum efficiency (s-EQE) and electroluminescence (EL) spectra using the classical Marcus theory in the high temperature limit with an assumption that the molecular vibrational energy is much lower than the thermal energy k_BT.[30,35] In this method, CT absorption and emission spectra can be fitted with two symmetric Gaussian functions, and eventually E_{CT} and λ can be extracted. This method is now routinely employed in OPV research.

Although the analysis based on the classical Marcus theory has achieved remarkable success in OPVs, its employment in current high-performance devices faces severe challenges. With the emergence of non-fullerene acceptors (NFAs), device efficiency has increased to over 20%, mainly due to a significant reduction in energetic offset and subsequently voltage loss.[36–41] Small offsets also lead to spectral overlap between locally excited (LE) and CT emissions; hence, the standard single-state Marcus analysis is subject to the overlapping interference from many complex factors. Consequently, the weak CT absorption signal is often masked by the steep absorption edge of the narrow band gap NFA, and the EL spectrum is dominated by the bright LE emission.[42–44] If the standard analysis method is directly applied to such spectra, the extracted value of E_{CT} would be close to E_{LE} and overestimated.

In addition, in systems with small energetic offset and strong electronic coupling, LE and CT states may be mixed to form hybrid states that do not conform to the simple Marcus model.[45,46] This hybridization between LE and CT states creates mixed electronic character that violates Marcus theory's discrete two-state model.[47–49] The degree of this hybridization depends on the ratio of electronic coupling strength to driving force: systems with moderate coupling strength and high driving force have a limited degree of hybridization (about 3%), while in systems where the driving force is close to zero, the hybridization effect is much more significant.[47] The LE–CT hybridization with mixed energy states fundamentally challenges Marcus theory. A three-state vibrational electron model that considers the coupling of electrons and vibrations with localized absorption states is crucial for reliably describing optical absorption characteristics, because the classical Marcus model leads to incorrect interpretation.[48] This hybridization results in an intensity borrowing mechanism that increases the oscillator strength of the effective CT to the ground state, hence suppressing nonradiative voltage losses, which cannot be explained by the classical Marcus theory alone.[49]

Finally, the organic semiconductor film itself has significant static energetic disorder, which further complicates the extraction of CT state properties.[50–52] The static disorder caused by irregular molecular packing and conformational changes in organic films leads to a distribution of CT state energies. Intermolecular interactions in organic blends exhibit weak cohesion through van der Waals forces, and combined with conformational irregularities, this results in a broadened distribution of charge transfer states.[53] Static energetic disorder is expected to be pronounced in amorphous organic semiconductors and in heterogeneous blended films commonly used in OPV devices.[54] However, classical Marcus theory assumes the existence of a single charge transfer energy level, with the broadening of its spectral features attributed solely to electron–phonon coupling (dynamic disorder).[55] Although traditional models can be extended to account for this phenomenon, the commonly applied classical Marcus approach neglects this effect.

In view of the above limitations and challenges, a practical guide on classical Marcus theory analysis of CT states is urgently needed in OPVs. If the existing model is directly applied without fully understanding its premise, it is easy to draw wrong conclusions. The purpose of this study is to first systematically integrate potential problems in classical Marcus analysis, and provide a unified diagnostic framework to elucidate how to carefully interpret the EL and s-EQE spectra under the framework of classical Marcus theory, with special attention to static disorder and the mixed LE and CT emission, in particular the invisible CT states in current NFA-based systems.

2 Basics of classical Marcus theory

Marcus theory provides a framework for calculating the electron transfer rate between two electronic states coupled to a dynamic nuclear environment.[10] The model takes into account the effects of intramolecular vibrations and surrounding molecular matrices. The core idea is that electron transfer is most likely to occur when the nuclear coordinate fluctuates to a configuration where the initial and final electron energies are equal, *i.e.*, a vertical transition. This condition conforms to the Franck–Condon principle and the electron transition is much faster

than the nuclear motion.[18,19] The theory uses a non-adiabatic potential energy surface to describe this process. It approximates the potential energy surface of the initial state and the final state to a simple harmonic potential with the same curvature. This parabolic approximation simplifies the geometry of the complex, multi-dimensional and possibly anharmonic potential energy surface in the real world. The key assumptions are as follows: first of all, the potential energy surfaces of the initial state and the final state have a quadratic dependence on the nuclear reaction coordinate; secondly, the response of the surrounding environment to charge rearrangement is linear, and the dielectric response changes proportionally. Thirdly, using the Condon approximation, it is assumed that the electron coupling matrix element H_{DA} is independent of the nuclear coordinates, so the transition probability is completely determined by the nuclear configuration. Finally, the model is applicable to the non-adiabatic limit (weak electronic coupling), and the system evolves along the initial potential energy surface until it jumps to the final potential energy surface at the crossover point.[24,56–58] This hypothesis is particularly consistent with the optically weak transition characteristics of charge transfer states in OPV blends.

For optical transitions involving CT states, it is usually necessary to consider two potential energy surfaces: one represents the ground state (GS) of the D–A pair, and the other represents the CT state (D^-–A^+). As shown in Fig. 1(a), these potential energy surfaces are plotted along a generalized one-dimensional "reaction coordinate". Within this parabolic framework, the kinetics and thermodynamics of the charge transfer process are described by several key parameters. For optical transitions of absorption and emission between the ground state and the CT state, the standard Gibbs free energy change ΔG^0 of the reaction is simply the energy difference between the two potential energy surface minima, *i.e.* the CT state energy E_{CT}. Reorganization energy λ is defined as the energy required to distort the nuclear geometry of the initial state (reactant plus the environment) to the equilibrium geometry of the final state without the occurrence of the electron transfer event itself. It is the vertical energy difference between the final state potential energy calculated at the equilibrium coordinates of the initial state and the minimum value of the final state potential energy. λ quantifies the energy dissipated during the instantaneous electron transfer when the nuclear coordinates of the system relax to their new equilibrium positions.[59–61] It includes two main contributions: the inner ring component (λ_i) caused by the change of intramolecular bond length and bond angle, and the outer ring component (λ_o) caused by the reorientation of the surrounding polarized medium. In the classical Marcus theory, only the outer reorganization energy is considered.[62] The activation energy $\Delta G^{\ddagger}$ for the transition is the energy of the crossing point of the two parabolas relative to the minimum of the initial state parabola.[10] A straightforward geometric derivation based on the parabolic approximation yields the Marcus equation for the free energy of activation:

$$\Delta G^{\ddagger} = \frac{(\lambda + \Delta G^0)^2}{4\lambda} \quad (1)$$

For the non-radiative recombination process from the CT state back to the ground state, the initial state is the CT state and the final state is the ground state. Therefore, the driving force is $\Delta G^0 = -E_{CT}$. The activation barrier for this loss pathway is thus given by:

$$\Delta G^{\ddagger}_{rec} = \frac{(\lambda - E_{CT})^2}{4\lambda} \quad (2)$$

Under the non-adiabatic limit and low frequency approximation, the rate of electron transfer (k_{ET}) is described by the classical Marcus expression:

$$k_{ET} = \frac{2\pi}{\hbar}|H_{DA}|^2 \frac{1}{\sqrt{4\pi\lambda k_B T}} \exp\left(-\frac{(\Delta G^0 + \lambda)^2}{4\lambda k_B T}\right) \quad (3)$$

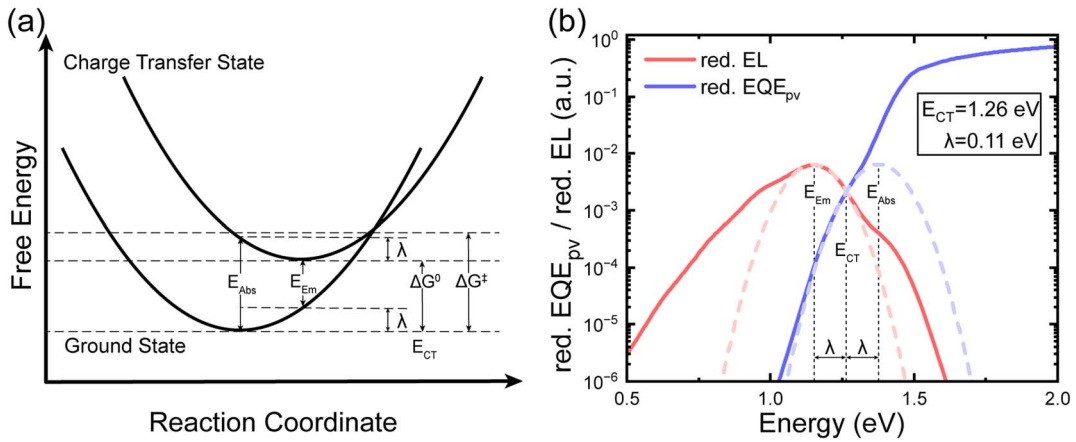

Fig. 1 (a) Schematic diagram of the evolution of potential energies for the ground state and charge transfer state along the reaction coordinate, for harmonic potentials. ΔG^0 represents the Gibbs free energy change of the reaction, and $\Delta G^{\ddagger}$ represents the activation barrier; (b) schematic diagram of Marcus theory fit of the reduced EQE_{PV} and EL spectra. In (a) and (b), E_{abs} and E_{em} represent the energies of maximum absorption and emission, respectively; E_{CT} represents to the charge transfer state energy, and λ represents the reorganization energy.

where $\hbar$ is the reduced Planck constant, $|H_{DA}|$ is the electronic coupling matrix element, k_B is the Boltzmann constant, and T is the absolute temperature. This quadratic dependence of the activation energy on ΔG^0 leads to the existence of a "normal" and an "inverted" region for reaction rates, suggesting that very large E_{CT} values could potentially suppress non-radiative recombination rates.

The processes of photon absorption and emission are visualized as vertical Franck–Condon transitions on the potential energy diagram. The absorption process involves a vertical transition from the equilibrium configuration (minimum) of the ground state parabola. This transformation terminates on the parabola of the CT state, and its energy is one λ higher than the minimum value of the CT state potential energy surface. Conversely, radiative recombination (emission) involves a vertical transition from the minimum of the CT state parabola down to the ground state parabola. Thus, the photon energies corresponding to the maximum absorption and emission intensity are approximately given by:

$$E_{abs} \approx E_{CT} + \lambda \tag{4}$$

$$E_{em} \approx E_{CT} - \lambda \tag{5}$$

The energy difference between the absorption and emission maxima is known as the Stokes shift, which provides an experimentally accessible spectroscopic handle for determining the reorganization energy:

$$\text{Stokes shift} = E_{abs} - E_{em} \approx 2\lambda \tag{6}$$

These key parameters correspond to EL and s-EQE data (reduced) fitted using the standard Marcus theory, as shown in Fig. 1(b).

In the high temperature limit, when the thermal energy (k_BT) is large relative to the energy of the relevant nuclear vibration mode ($\hbar\omega$), the thermal population of the initial vibrational energy levels leads to the Gaussian broadening of the optical transition.[30,35] Therefore, the absorption $A(E)$ and emission $N(E)$ line shapes will be Gaussian, centered on E_{abs} and E_{em}, respectively:

$$A(E) \propto E \exp\left(-\frac{(E-(E_{CT}+\lambda))^2}{4\lambda k_B T}\right) \tag{7}$$

$$N(E) \propto E^3 \exp\left(-\frac{(E-(E_{CT}-\lambda))^2}{4\lambda k_B T}\right) \tag{8}$$

3 Standard procedure of Marcus analysis

Marcus analysis requires simultaneous investigation of the absorption and emission spectra of the CT state. The theoretical basis of this method is derived from the detailed balance principle under thermal equilibrium conditions: in the thermal equilibrium state, the forward rate of any microscopic process is equal to its reverse rate. For optical transitions, this principle establishes a relationship between the absorption and emission spectrum, which was originally proposed by Kennard and Stepanov.[63–65] In the context of a solar cell, this principle is formalized in an electro-optical reciprocity relation, which connects the device's photovoltaic quantum efficiency (EQE_{PV}) to its electroluminescence emission photon flux density (ϕ_{em}):[66,67]

$$\phi_{em}(E) = EQE_{PV}(E) \times \phi_{BB}(E,T)\left[\exp\left(\frac{qV}{kT}\right) - 1\right] \tag{9}$$

where $\phi_{BB}(E,T)$ is the spectral flux density of a blackbody radiator at absolute temperature T, and V is the applied voltage. This equation elegantly links the process of absorbing a photon to generate an electron–hole pair (probed by EQE_{PV}, assuming $EQE_{PV} \approx A(E)$) with the reverse process of an electron–hole pair recombining to emit a photon (probed by $N(E)$,[50] *i.e.* the number of photons collected for a given time duration and device area; hence $N(E) \propto \phi_{em}(E)$).

For the analysis, the highly sensitive $EQE_{PV}(E)$ spectrum and EL intensity spectrum $N(E)$ of the solar cell device are first carefully measured. Once obtained, the reduced absorption spectrum is calculated by dividing the measured EQE_{PV} by the photon energy E resulting in a quantity proportional to the absorption cross-section:

$$\text{red. } EQE_{PV}(E) = \frac{EQE_{PV}(E)}{E} \tag{10}$$

Similarly, the reduced emission spectrum is mirrored to the reduced absorption spectrum:

$$\text{red. } EL(E) = \frac{N(E)}{E^3} \tag{11}$$

The manual fitting process requires judgment of visual features such as curve trend, peak position and line width, and normalization of red. $EQE_{PV}(E)$ and red. $EL(E)$ is required. After this processing, the two reduced spectra are ready for quantitative fitting, as depicted in Fig. 2(a).

In the large offset case, the CT absorption and emission characteristics can be clearly separated from the LE transition in the spectrum, showing obvious peaks or tails in the sub-band gap region, as shown in Fig. 2(a). This spectral separation effectively avoids the complexity caused by the overlap of absorption bands, so that we can directly and clearly fit the characteristics of the CT state. The reduced absorption and emission spectra are then fitted using the Gaussian line shapes derived from the classical Marcus theory, respectively:

$$\text{red. } EQE_{PV}(E) = \frac{A}{\sqrt{4\pi\lambda k_B T}} \times \exp\left(-\frac{(E-(E_{CT}+\lambda))^2}{4\lambda k_B T}\right) \tag{12}$$

$$\text{red. } EL(E) = \frac{B}{\sqrt{4\pi\lambda k_B T}} \times \exp\left(-\frac{(E-(E_{CT}-\lambda))^2}{4\lambda k_B T}\right) \tag{13}$$

where A and B are independent amplitude scaling factors and are proportional to the square of the electronic coupling matrix element.

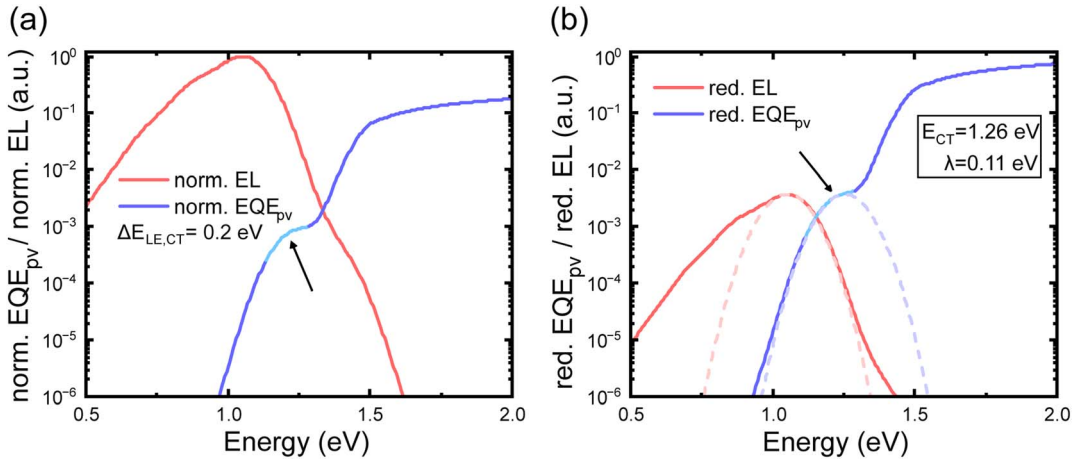

Fig. 2 Schematic diagram of the steps involved in fitting EL and EQE spectra using Marcus theory. (a) The first step is to normalize the experimental EL and EQE data. A clear CT absorption peak (the bright blue curve segment) is observed in the normalized EQE_{PV} (norm. EQE_{PV}) curve. (b) The second step is to shift the main peak of the reduced electroluminescence (red. EL) spectrum downward so that its intensity matches with the CT peak in the reduced EQE_{PV} (red. EQE_{PV}) spectrum. The dashed Gaussian line represents the fitting result based on classical Marcus theory.

When performing global fitting on the normalized data, the red.EL curve is usually shifted downward so that the peak height of red.EL matches that of the CT peak in the red.EQE_{PV} curve, and E_{CT} and λ are constrained as shared parameters for absorption and emission line shapes. The position and width of the absorption peak (centered at $E_{CT} + \lambda$) and the emission peak (centered at $E_{CT} - \lambda$) are simultaneously described through a set of self-consistent physical parameters, as shown in Fig. 2(b). This approach takes advantage of the inherent mirror symmetry predicted by the theory, and compared with fitting a single spectrum separately, it can obtain more reliable E_{CT} and λ values. Among them, E_{CT} reflects the energy of the interfacial CT state after relaxation, which is the main factor determining the thermodynamic limit of V_{oc},[68,69] and non-radiative voltage loss ($V_{loss,nr}$).[22,70] λ indicates the extent to which nuclei and electrons reorganize at the donor–acceptor interface after a charge transfer event occurs. Smaller reorganization energies are preferred because less energy is lost due to structural relaxation. In addition, smaller λ is often associated with steeper absorption edges, hence less dynamic disorder.

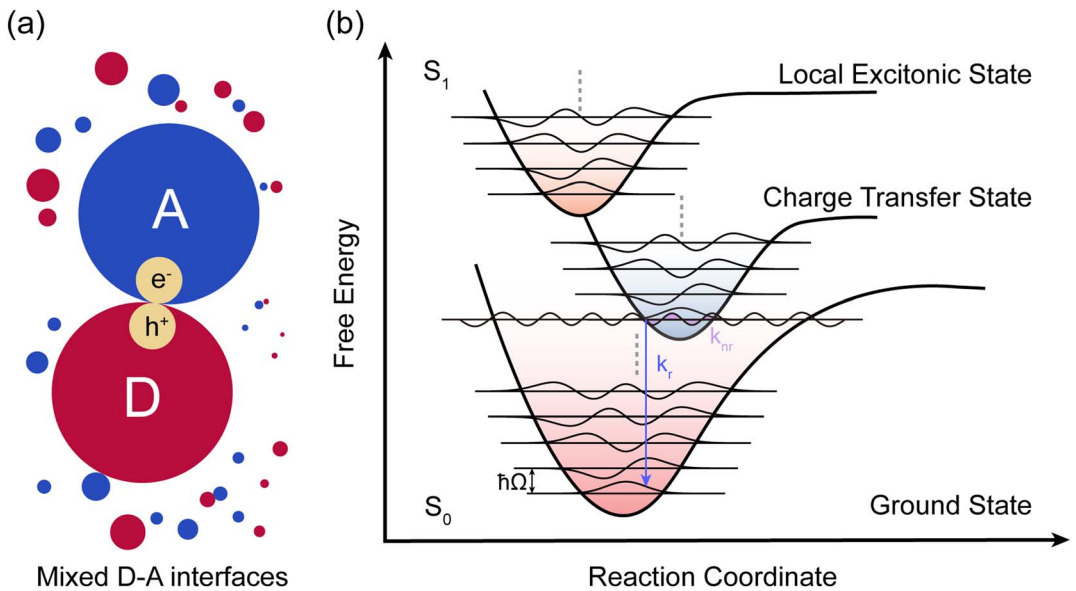

Fig. 3 (a) Schematic diagram of an electron and a hole occupying the interfacial CT states at the junction of the donor domain (red) and the acceptor domain (blue); (b) the potential energy surface plot depicts the evolution of potential energies for the ground state, charge transfer state, and local excitonic state along the reaction coordinate. The ground state is shown in red, the local excitonic state is shown in orange, and the charge transfer state is shown in blue. Blue arrows indicate radiative decay pathways, while the pink shaded area (indicating the overlap between the vibrational modes of the lowest CT state and those of the highest ground state) represents non-radiative recombination pathways.

4 Systems with complex absorption and emission spectra

The absorption and emission spectra of a typical bulk heterojunction (BHJ) OPV are determined by various properties of CT states. In the case of traditional large offset systems (typically >0.3 eV), *e.g.* most fullerene based systems, we can clearly see emissions from CT states, making it straightforward to conduct single-state classical Marcus analysis.[30] However, state-of-the-art NFA systems often feature a small offset (typically <0.2 eV), leading to possibilities of thermal repopulation[71] and state hybridization.[48,49] Besides, organic semiconductors have intrinsic static energetic disorder that may arise from configurational disorder and packing disorder, which are strongly correlated to the nanoscale interpenetrating network of donors and acceptors, as shown in Fig. 3(a). In this part, we will discuss the validity of single-state Marcus analysis when absorption and emission spectra are complex.

We employ a previously developed model framework based on the semi-classical Marcus theory[49,50,70,72] to generate a synthetic database of EQE_{PV} and EL spectra as inputs for the subsequent Marcus analysis (Note S1). This model generates spectra with complex features of CT states, including static energetic disorder, state hybridization, dark CT, *etc.*, which allows us to fully explore the accuracy of E_{CT} and λ based on the standard Marcus analysis in the case of complex emission spectra. The framework describes the transitions between the ground state (GS or S_0), the localized exciton (LE or S_1) state and the CT state, as shown in the potential energy surface in Fig. 3(b). Based on the semi-classical Marcus–Levich–Jortner (MLJ) theory, the model decomposes the reorganization energy into low-frequency (λ_o) and high-frequency components (λ_i). The low-frequency components, after classical processing, correspond to solvent/matrix relaxation and low-frequency vibration, while the high-frequency components correspond to the dominant quantum mechanical vibration mode with an energy of $\hbar\Omega$.[70] The MLJ expression of the non-radiative rate constant k_{nr} is given by the sum of Franck–Condon weighted densities of states:

$$k_{nr} = \frac{2\pi {V_{el}}^2}{\hbar\sqrt{4\pi\lambda_o k_B T}} \sum_{m=0}^{\infty}\sum_{n=0}^{\infty} \frac{e^{-S} S^{m-n} n!}{m!} [{L_n}^{m-n}(S)]^2 \, e \left\{ - \frac{[-\hbar\omega + E_{CT} + \lambda_o + (m-n)\hbar\Omega]^2}{4\lambda_o k_B T} \right\} e^{-\frac{n\hbar\Omega}{k_B T}} \quad (14)$$

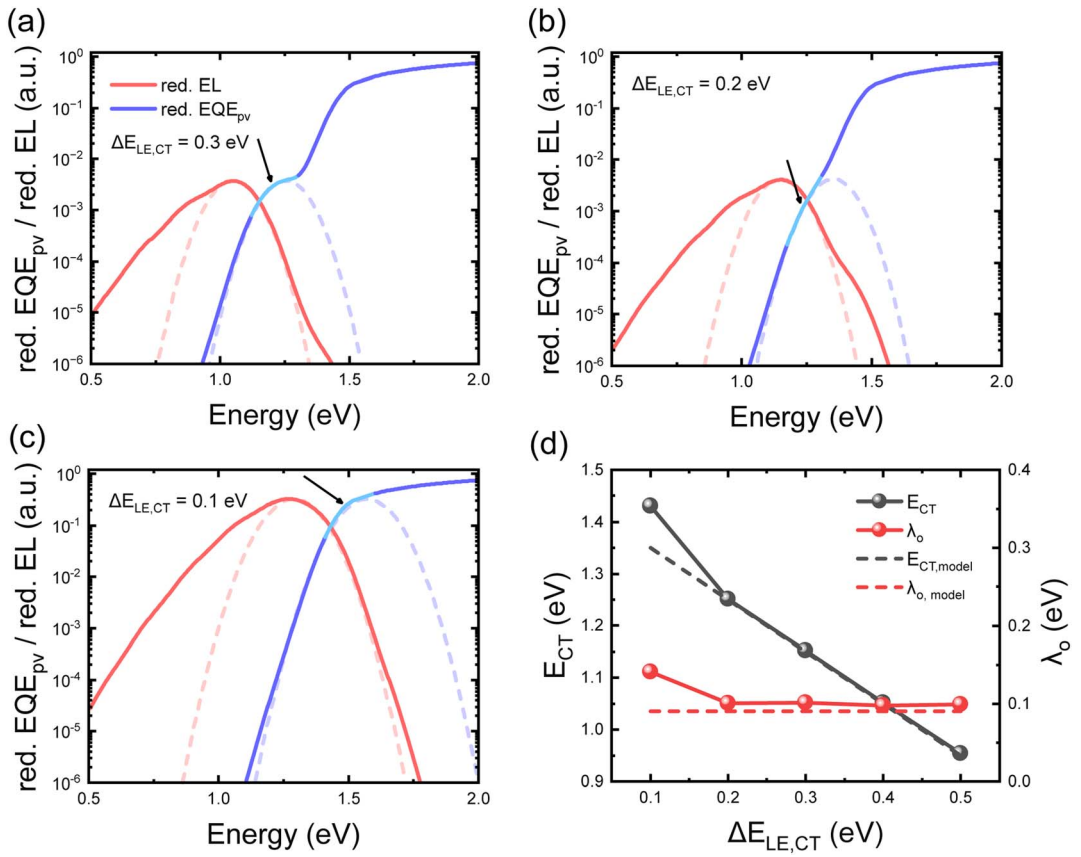

Fig. 4 Summary of the results for different offsets ($\Delta E_{LE,CT}$) *via* fitting EL and EQE spectra using the classical Marcus theory. When performing Marcus fitting on the results with offsets of (a) 0.3 eV, (b) 0.2 eV, and (c) 0.1 eV, the bright blue curve segment is a reference marker indicating the downward shift of the main peak of the red. EL spectrum. (d) Comparison between the physical parameters of the original model and the classical Marcus fit results. The previously developed model[49,50,70,72] was used to generate EL and EQE data, with input parameters as shown in Note S1. The dotted line represents the parameters set in the original model, and the solid line represents the result obtained by the classical Marcus fitting. $\lambda_{o,model}$ corresponds to the low frequency reorganization energy of the CT state in the original model, and $E_{CT,model}$ corresponds to the free energy of the CT state.

Here, V_{el}^2 is the electronic coupling between the CT and ground states, $S = \lambda_i/\hbar\Omega$ is the Huang–Rhys factor, m and n designate the quantum number of the vibrational modes of the final and initial state, respectively, and $L_n^{m-n}(S)$ is the generalized Laguerre polynomial of degree n.

Another key component of this model is the state hybridization between LE and CT states, which becomes significant when the offset between them is small (usually <0.2 eV).[49] This interaction is mediated by an electron coupling matrix element (V_{star}), resulting in state mixing and the formation of new hybrid states. A major consequence is the "intensity borrowing", where a new low-energy state, mainly the CT-like state, obtains a small part of the large oscillator strength of the "bright" LE state. This greatly improves the effective oscillator strength of CT to GS transition:

$$f^*_{GS,\,CT} = f_{GS,CT} + \frac{f_{LE,GS}\,V_{star}^2}{\Delta E_{LE,CT}^2} + \frac{2\sqrt{f_{LE,GS} f_{GS,CT}}\,V_{star}}{\Delta E_{LE,CT}} \quad (15)$$

This formula shows that the effective oscillator strength increases substantially as the energy offset ($\Delta E_{LE,CT}$) decreases and V_{star} increases. This "brighter" CT state directly increases the radiative recombination rate k_r.

Static energetic disorder is also a key component in this model.[50] The CT state is described by a normalized distribution function for CT-state energies $g(E_{CT})$, which is the sum of multiple weighted Gaussian line-shapes $D_t(E_{CT})$, *via* $g(E_{CT}) = \sum_t c_t D_t(E_{CT})$. For an individual Gaussian function, $\sigma_{CT,t}$ is its width and $E_{CT,t}$ is the energy at its Gaussian center:

$$D_t(E_{CT}) = \frac{1}{\sigma_{CT,t}\sqrt{2\pi}}\, e^{-\frac{\left(E_{CT} - \langle E_{CT,t}\rangle\right)^2}{2\sigma_{CT,t}^2}} \quad (16)$$

The parameter $\sigma_{CT,t}$ quantifies the degree of static disorder for an individual CT manifold t. This is the main cause of the broadening of the low-energy tail in the absorption and emission spectra. Ignoring this distribution will cause the fitting routine to wrongly attribute spectral broadening to artificially exaggerated λ. Because k_{nr} is highly sensitive to λ, it may lead to a significant misjudgment of the recombination rates. Note here that for brevity, we consider a single Gaussian DOS for later investigations; therefore, the subscript "t" is neglected.

We now study the systematic influence of key physical parameters on the accuracy of classical Marcus analysis,

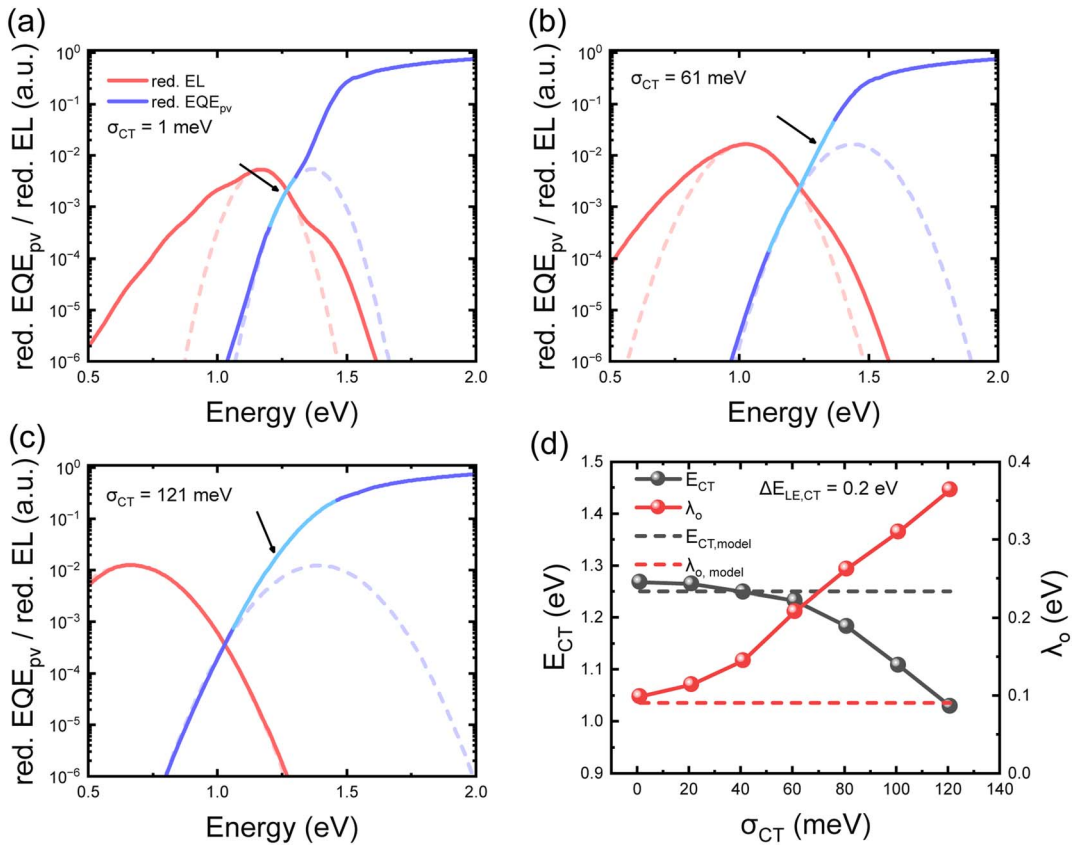

Fig. 5 Summary of the results for different static disorder (σ_{CT}) with $\Delta E_{LE,CT}$ = 0.2 eV *via* fitting EL and EQE spectra using the classical Marcus theory. When performing Marcus fitting on the results with static disorder of (a) 1 meV, (b) 61 meV, and (c) 121 meV, the bright blue curve segment is a reference marker indicating the downward shift of the main peak of the red. EL spectrum. (d) Comparison between the physical parameters of the original model and the classical Marcus fit results. The previously developed model was used to generate EL and EQE data, with input parameters as shown in Note S1. The dotted line represents the parameters set in the original model, and the solid line represents the result obtained by the classical Marcus fitting. $\lambda_{o,model}$ corresponds to the low frequency reorganization energy of the CT state in the original model, and $E_{CT,model}$ corresponds to the free energy of the CT state.

including the offset between the LE and CT states ($\Delta E_{LE,CT}$), static disorder of CT states (σ_{CT}), coupling between the LE and CT states (V_{star}), low and high frequency reorganization energy of the CT state (λ_o and λ_i), CT oscillator strength ($f_{osc.CT}$), and the rate constant of the LE to CT transition ($k_{LE,CT}$), as shown in Table S1. The model parameters used to generate EL and EQE spectra are shown in Table S2. By fitting these simulated spectra using the homemade Marcus theory-based program *Marcusfit*[73] (Note S2), we can directly compare the fitting parameters (E_{CT} and λ_o) with the known "true" values in the model. $\lambda_{o,model}$ and $E_{CT,model}$ correspond to the low frequency reorganization energy and the free energy of the CT state in the original model, respectively. This analysis reveals several key scenarios where the classical Marcus analysis fails as shown in Fig. 4–9 and detailed below.

4.1 Low offset

We first investigate the case where the LE–CT offset ($\Delta E_{LE,CT}$) is reduced, which is a typical approach to minimize voltage loss experimentally. As shown in Fig. 4(a and b), for large offset systems ($\Delta E_{LE,CT} \geq 0.2$ eV), a distinct CT peak (the bright blue curve segment) can be observed at the tail of the EQE curve, and E_{CT} and λ_o from Classical Marcus fitting agree reasonably well with the input model values, as shown in Fig. 4(d). In contrast, for small offset systems (*e.g.* $\Delta E_{LE,CT} = 0.1$ eV in Fig. 4(c)), due to spectral overlap, the EQE tail represents a mixture of CT and LE absorption, and no clear CT absorption or emission is visible. Since the oscillator strength of the LE state is usually much larger than that of the CT state, the classical Marcus fit often only captures features of the LE state, leading to overestimated E_{CT} and λ_o due to overlapped emission, as shown in Fig. 4(d). Later, we will show that such results are typical for low offset systems when other properties of CT states change.

4.2 Large static disorder

We now investigate the case of varying static energetic disorder in CT states, *i.e.* σ_{CT}. As shown in Fig. 5(a–c), for $\Delta E_{LE,CT}$ is fixed at 0.2 eV (moderate offset), the breadth of both EL and EQE increases with increasing static disorder. The Gaussian line shape of the single-state Marcus model results from uniform broadening caused by vibrational electron–phonon coupling. Static disorder, that represents the statistical distribution of molecular site energy due to morphological changes and the local electrostatic environment, introduces non-uniform broadening by creating a Gaussian density of states (DOS) for excited states. Therefore, the emission spectrum observed in the experiment is a convolution of the intrinsically uniform line shape with this non-uniform DOS. Under thermal equilibrium, excitons undergo thermal relaxation and migrate to lower-energy positions within the DOS before emission. This process causes the emission spectrum to shift to the lower energy side, resulting in a wide, asymmetric non-Gaussian distribution in EL, that cannot be easily analyzed by single state Marcus theory. As shown in Fig. 5(d), for systems with low disorder ($\sigma_{CT} < 60$ meV), only E_{CT} values are roughly recovered by Marcus fitting, while λ_o deviates significantly from input values, $\lambda_{o,model}$. For large static disorder systems, the fitted E_{CT} is systematically severely underestimated due to exciton relaxation in the DOS, in which case the values of E_{CT} can only be considered as the effective value of CT manifolds,[74] rather than the center of CT DOS. In the case of high disorder ($\sigma_{CT} = 120$ meV), the deviation exceeds 0.2 eV. Therefore, λ_o values extracted directly using classical Marcus theory are seriously overestimated. A similar observation is seen with a smaller offset ($\Delta E_{LE,CT} = 0.1$ eV), as shown in Fig. S1(c).

4.3 Strong state hybridization

We now investigate the case with varied electronic coupling (from 0 meV to 80 meV) between the LE and CT states (V_{star}), where $\Delta E_{LE,CT}$ is fixed at 0.1 eV. When the electronic coupling between LE and CT state rises, there is no longer pure CT or LE state, but rather a combination of both, *i.e.* a hybrid state. LE states typically exhibit large oscillator strength $f_{LE,GS}$, whereas the oscillator strength of pure CT states (*i.e.* $f_{GS,CT}$) is usually several orders of magnitude lower than that of LE.[49] According to eqn (15), even a small amount of LE component mixed into the CT state leads to a dramatic increase in the effective oscillator strength of the CT state; hence, the change in $f_{GS,CT}$ is the key factor here.

As shown in Fig. 6(a–c), the fitting quality of the classical Marcus theory gradually improves with increasing V_{star}. When V_{star} is small (weak coupling), the CT state cannot acquire sufficient transition dipole moments from the LE state, which renders it intrinsically an optical "dark state". This case is equivalent to the low offset case discussed above, and the classical Marcus fit only captures the LE state's tail characteristics rather than the true CT state. Consequently, the extracted E_{CT} and λ_o values are incorrectly biased toward the higher-energy LE state, as shown in Fig. 6(d). Conversely, when V_{star} becomes larger (intermediate coupling, *e.g.* 80 meV), the intensity borrowing effect is activated.[49] The CT state gains substantial oscillator strength, transforming into a "bright state" and forming an independent, distinct absorption peak or shoulder peak, which leads to slightly better fitting quality, as reflected in Fig. 6(a–c), and reduced fitting errors in Fig. 6(d). However, it's worth noting here that in all cases when the offset is small, noticeable errors appear using the classical Marcus fit, reflecting the results from discussions above. Such behavior is absent in larger offset systems, *e.g.* 0.2 eV in Fig. S1(g).

Note that we are still in the weak to intermediate coupling regime ($V_{star} < 0.5\lambda$);[75] therefore, Fermi's Golden rule and the parabolic potential energy surface can still be applied, given that the offset between the LE and CT state is not smaller than 50 meV.[49] For strong coupling with $V_{star} > 0.5\lambda$ and $\Delta E_{LE,CT} < 50$ meV, the parabolic potential energy surface is no longer applicable, and a correction on the wavefunction of the CT state is needed, which is beyond the scope of the current work.[76]

4.4 High reorganization energies

We turn to investigate the case with different low and/or high frequency reorganization energy ($\lambda_{o,model}$ and/or $\lambda_{i,model}$) of CT states. For a clearer presentation, we fix the values for $\lambda_{i,model}$,

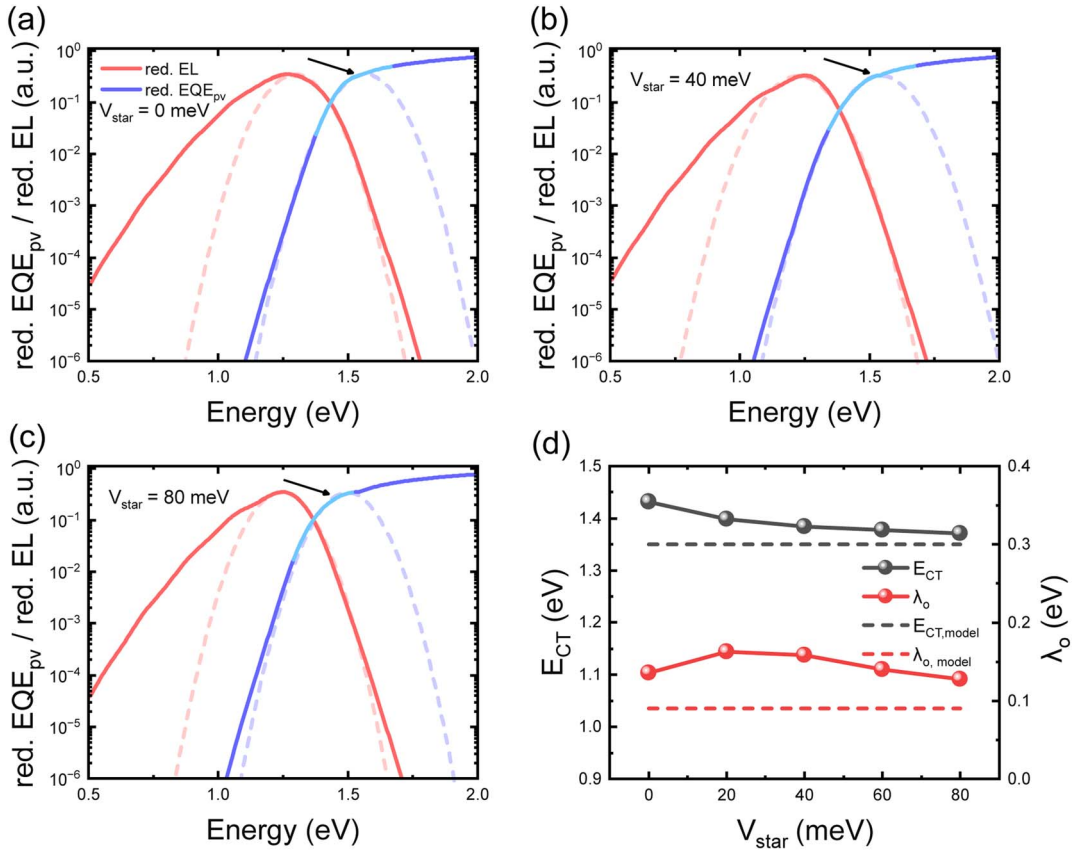

Fig. 6 Summary of the results for different state hybridization (V_{star}) with $\Delta E_{LE,CT} = 0.1$ eV *via* fitting EL and EQE spectra using the classical Marcus theory. When performing Marcus fitting on the results with state hybridization of (a) 0 meV, (b) 40 meV, and (c) 80 meV, the bright blue curve segment is a reference marker indicating the downward shift of the main peak of the red. EL spectrum. (d) Comparison between the physical parameters of the original model and the classical Marcus fit results. The previously developed model was used to generate EL and EQE data, with input parameters as shown in Note S1. The dotted line represents the parameters set in the original model, and the solid line represents the result obtained by the classical Marcus fitting. $\lambda_{o,model}$ corresponds to the low frequency reorganization energy of the CT state in the original model, and $E_{CT,model}$ corresponds to the free energy of the CT state.

and vary $\lambda_{o,model}$, and finally compare the extracted λ_o with input values of $\lambda_{o,model}$, as shown in Fig. 7. We consider three cases with small (60 meV), medium (90 meV), and large (120 meV) $\lambda_{i,model}$ values for the generation of EL and EQE spectra.

For spectral fitting, it can be observed that with $\Delta E_{LE,CT} = 0.2$ eV, a distinct CT peak can be visually identified at the tail of EQE in all cases, as shown in Fig. 7. This provides a reliable reference for extracting E_{CT} and λ_o, leading to good agreement when $\lambda_{o,model}$ is small. However, when $\lambda_{o,model}$ rises, the extracted E_{CT} and λ_o values tend to be overestimated. This occurs because as $\lambda_{o,model}$ increases, the CT spectrum widens and extends toward higher energies due to broadening caused by λ_o, significantly increasing the overlap with the LE state. To fit the blended spectral edges, the Gaussian function is forced to shift toward higher energies with a widened distribution, leading to artificially inflated E_{CT} and λ_o values for all cases with different input values of $\lambda_{i,model}$, as shown in Fig. 7(d,h and l). Larger $\lambda_{i,model}$ tends to lead to larger errors due to additional broadening caused by vibronic modes.

In the system with $\Delta E_{LE,CT} = 0.3$ eV, *i.e.* a larger offset, the CT state exhibits spectral characteristics that are well separated from the LE state. Therefore, regardless of how the reorganization energy changes in this scenario, classical Marcus theory can accurately extract E_{CT}, as shown in Fig. S1(d–f). In the MLJ model, the emission exhibits a spectral envelope composed of a series of subpeaks spaced by high-frequency vibrational energy levels ($\hbar\omega \approx 0.15$–0.2 eV), where each subpeak's width is determined solely by λ_o and σ_{CT}.[50] When fitting this multi-peak structure using the single Gaussian Marcus theory, the algorithm tends to match the shape of the strongest 0–0 transition main peak. Consequently, the extracted λ_o mainly reflects the $\lambda_{o,model}$ determining the main peak width, while "neglecting" the $\lambda_{i,model}$ that governs the relative intensity of the subpeaks. This explains the good agreement for large offset cases.

In the system with $\Delta E_{LE,CT} = 0.1$ eV, *i.e.* a small offset, as shown in Fig. S1(e and f), the extracted E_{CT} is ~0.07 eV larger than the model value. This is due to the strong spectral overlap between LE and CT states, and the classical Marcus fitting effectively fits the signal from the LE state, yielding an energy value consistently larger than E_{CT} but slightly less than E_{LE}. Thus, the fitted energy at this point actually represents the energy of the mixed LE and CT states. Additionally, the extracted reorganization energy tends to respond weakly to variations

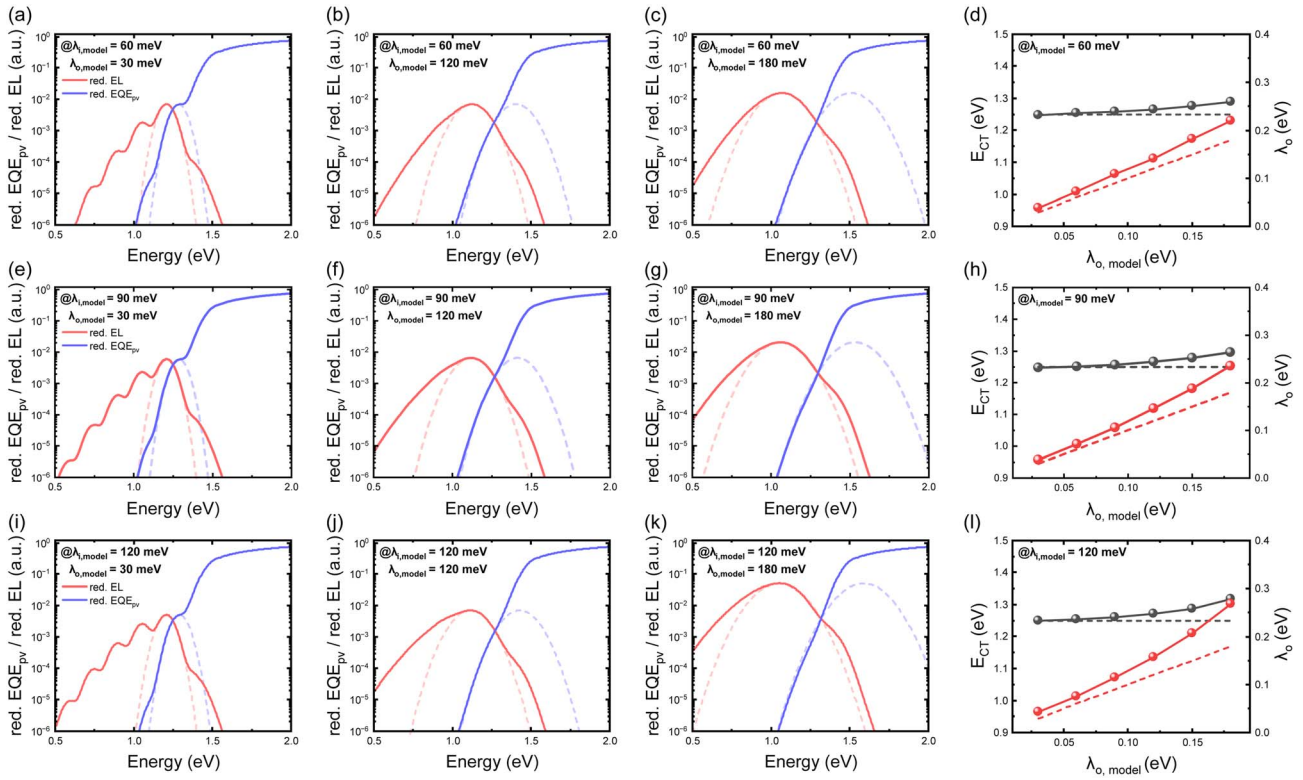

Fig. 7 Summary of the results for different CT low and/or high frequency reorganization energies (λ_o and/or λ_i) with $\Delta E_{LE,CT} = 0.2$ eV *via* fitting EL and EQE spectra using the classical Marcus theory. Input values ($\lambda_{i,model}$ and $\lambda_{o,model}$) for the model for generating EL and EQE spectral data are fixed as (a–d) $\lambda_{i,model} = 60$ meV; (e–h) $\lambda_{i,model} = 90$ meV; (i–l) $\lambda_{i,model} = 120$ meV with different $\lambda_{o,model}$. (d), (h), and (l) Comparison between the physical parameters of the original model and the classical Marcus fit results. The previously developed model was used to generate EL and EQE data, with input parameters as shown in Note S1. The dotted line represents the parameters set in the original model, and the solid line represents the result obtained by the classical Marcus fitting. $\lambda_{o,model}$ corresponds to the low frequency reorganization energy of the CT state in the original model, and $E_{CT,model}$ corresponds to the free energy of the CT state.

in the model reorganization energy. Therefore, the extracted λ_o reflects properties of the mixed LE and CT state, rather than the interfacial CT state. Consequently, regardless of how drastically the model alters the CT state's $\lambda_{o,model}$, as long as these changes do not significantly alter the dominance of the LE state, the values fitted by classical Marcus theory remain "inert". This further demonstrates that in systems with small offsets, the direct application of classical Marcus theory is questionable.

4.5 Low oscillator strength

We now investigate the case with different CT oscillator strengths ($f_{osc.CT}$). As shown in Fig. 8(a), for cases with $\Delta E_{LE,CT}$ fixed at 0.2 eV, under low oscillator strength conditions ($f_{osc.CT} = 5 \times 10^{-5}$), the CT state is essentially an optically "dark" state with an extremely low radiative transition rate. Since the intrinsic radiative rate of the LE state is typically several orders of magnitude higher than that of the "dark" CT state, LE emission tends dominate the EL spectrum. Consequently, the observed EL peak is located at the higher-energy LE position rather than the CT position. Therefore, the extracted E_{CT} is erroneously anchored near the LE state's energy, resulting in values significantly higher than the model input CT energy, similar to the low-offset cases. When the oscillator strength increases (*e.g.*, $f_{osc.CT} \geq 5 \times 10^{-3}$, Fig. 8(c)), clear CT absorption and emission features appear in the EQE tail and EL spectrum, respectively. In this case, the classical Marcus analysis is reasonable, resulting in extracted E_{CT} values that align well with model inputs. Interestingly, λ_o extracted using the classical Marcus theory does not vary with $f_{osc.CT}$ like E_{CT} does, as shown in Fig. 8(d). The fitting results remain consistently close to the model reorganization energy values, since we assume identical LE and CT properties apart from their oscillator strengths. For a different $\lambda_{o,model}$ value of the LE state, changes in λ_o can be expected. The large deviation observed when $f_{osc.CT} = 5 \times 10^{-3}$ is due to spectral overlap between LE and CT, leading to a broadened emission spectrum. Similar behavior is seen for smaller offsets, but not for large-offset cases due to good spectral isolation of the CT state from the LE state, as shown in Fig. S1(a).

Furthermore, we investigate the threshold of I_{CT}/I_{LE}, beyond which the Marcus analysis becomes meaningful. As shown in Fig. S2, when I_{CT}/I_{LE} is less than 8 folds, the extracted E_{CT} and λ values deviate significantly from the true values. During fitting, it becomes increasingly difficult to obtain good fitting results for the broadening of the CT peak and the intersection of the EL and EQE experimental data curves as I_{CT}/I_{LE} decreases. When

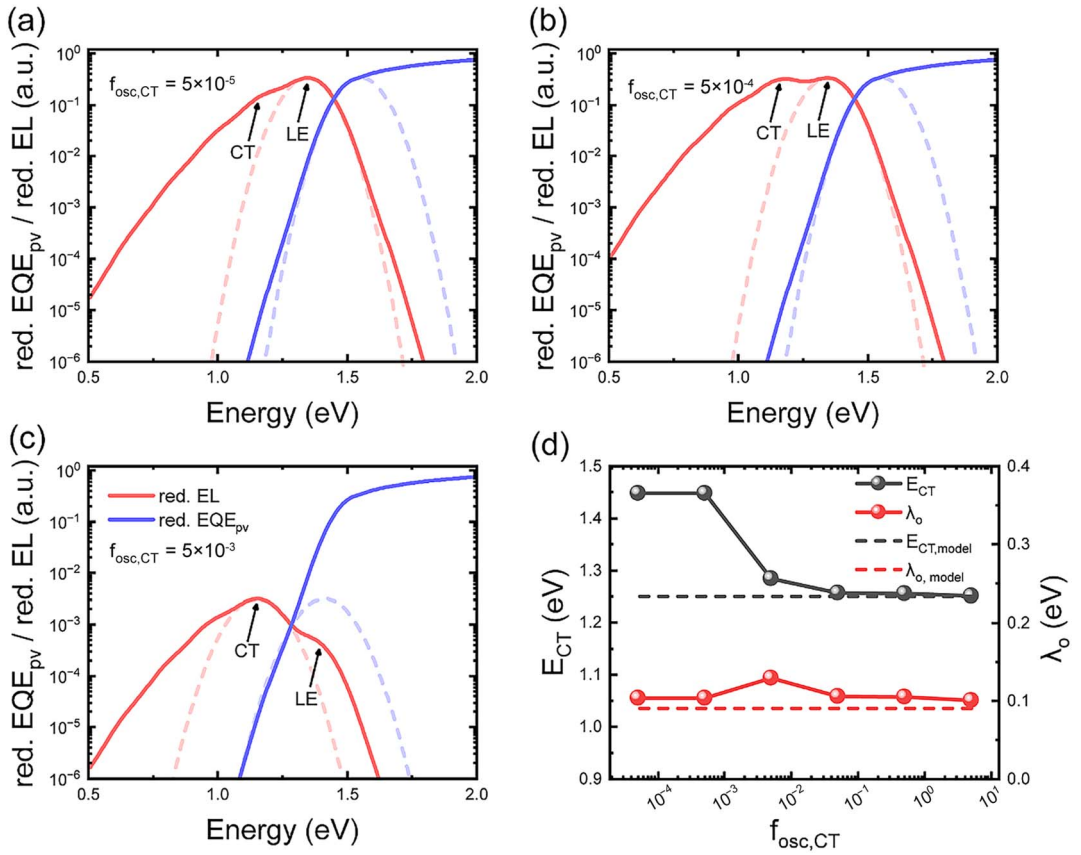

Fig. 8 Summary of the results for different CT oscillator strengths ($f_{osc,CT}$) with $\Delta E_{LE,CT} = 0.2$ eV *via* fitting EL and EQE spectra using the classical Marcus theory. (a–c) Fits obtained using an $f_{osc,CT}$ of 5×10^{-5}, 5×10^{-4}, and 5×10^{-3}, respectively. (d) Comparison between the physical parameters of the original model and the classical Marcus fit results. The previously developed model was used to generate EL and EQE data, with input parameters as shown in Note S1. The dotted line represents the parameters set in the original model, and the solid line represents the result obtained by the classical Marcus fitting. $\lambda_{o,model}$ corresponds to the low frequency reorganization energy of the CT state in the original model, and $E_{CT,model}$ corresponds to the free energy of the CT state.

the intensity ratio is too small ($I_{CT}/I_{LE} < 1$), the fitting obtained by forcibly fitting the CT peak is very poor (regardless of how the Marcus fitting parameters are adjusted), while the fitting of the LE peak demonstrates a better visual agreement. Therefore, if the high energy tail of the CT emission is visible with a peak intensity approximately one order of magnitude larger than that from LE states, classical Marcus analysis could lead to meaningful results; otherwise, it should be abandoned.

4.6 Low charge transfer rate

We finally investigate the case with different rate constants for the LE to CT transition ($k_{LE,CT}$). When $k_{LE,CT}$ is very large (*e.g.*, 10^{11} s^{-1}), as shown in Fig. 9(a) for cases where $\Delta E_{LE,CT}$ is fixed at 0.1 eV, electron transfer is considered to be efficient from LE to C, as is the back transfer rate from CT to LE, since CT is populated first in EL experiments. This leads to significant contributions from LE emission to the overall emission spectrum. When this happens, spectral interference from LE again becomes the central problem in the classical Marcus analysis; hence E_{CT} and λ_o are both overestimated, as also discussed above. At lower rates ($k_{LE,CT} \leq 10^9$ s^{-1}), however the fitted E_{CT} actually approaches the model predictions, as shown in Fig. 9(d). A lower $k_{LE,CT}$ indicates hindered charge transfer from LE to CT, and hence its back transfer from CT to LE. During EL experiments, this means electrically populated CT excitons tend to stay at CT rather than transferring back to LE. At this point, the dominant component of the EL spectrum may shift from LE to CT state emission, leading to much fewer errors in E_{CT}. The reorganization energy λ_o consistently shows an overestimation, due to the fitting of the mixed CT and LE state emission. Such behavior is, however, not seen for cases with large offsets, *i.e.* $\Delta E_{LE,CT} \geq 0.2$ eV, since the CT state will be much more populated than the LE state following Boltzmann statistics. Therefore, regardless of $k_{LE,CT}$, as long as CT state luminescence is observed, Marcus fitting can relatively accurately extract parameters, as shown in Fig. S1(b). This further exemplifies the key role of offset in performing the classical Marcus analysis.

5 Methods to avoid errors

As discussed above, the invisibility and inherent static disorder of CT states are two of the most important issues for standard single-state Marcus analysis. In particular, the invisible CT state is a common feature in the most efficient OPVs based on NFAs.

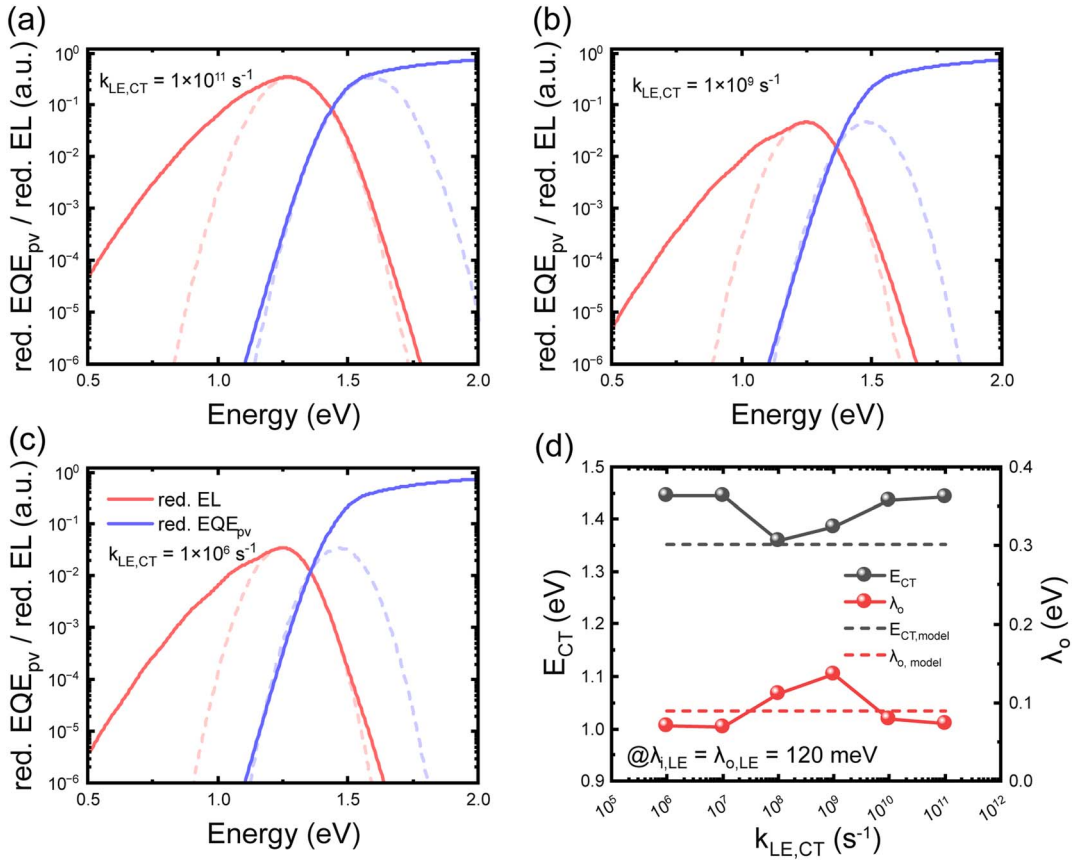

Fig. 9 Summary of the results for different rate constants of LE to CT states ($k_{LE,CT}$) with $\Delta E_{LE,CT} = 0.1$ eV *via* fitting EL and EQE spectra using the classical Marcus theory. (a–c) Fits obtained using $k_{LE,CT}$ values of 10^{11}, 10^{9}, and 10^{6} s^{-1}, respectively. (d) Comparison between the physical parameters of the original model and the classical Marcus fit results. The previously developed model was used to generate EL and EQE data, with input parameters as shown in Note S1. The dotted line represents the parameters set in the original model, and the solid line represents the result obtained by the classical Marcus fitting. $\lambda_{o,model}$ corresponds to the low frequency reorganization energy of the CT state in the original model, and $E_{CT,model}$ corresponds to the free energy of the CT state.

Here we distinguish two cases: (1) visible or partially visible CT states, *i.e.* the case when CT absorption or emission signals are visible or partially visible and not completely missing; (2) invisible CT states, *i.e.* the case when CT absorption and emission are completely covered by LE states. We suggest several alternative approaches to measure CT properties when absorption and emission signals are weak from CT states, and provide useful guides to quantitative analysis of CT states.

5.1 Visible or partially visible CT states

When emission or absorption signals from the CT state are not completely covered by LE states, we can still perform the classical Marcus analysis, but with a modified model considering static disorder. Here we discuss two methods that were proposed in the literature, as follows.

5.1.1 Temperature dependent sensitive EQE. The first method involves a temperature change during the optoelectronic experiment, *e.g.* temperature-dependent s-EQE as explored by Khan and Rand *et al.*[52] The benefit of the temperature dependent EQE experiment is that the absorption process doesn't involve exciton relaxation in the DOS, hence reducing errors due to unequilibrated excitons that might occur in temperature dependent luminescence experiments. However, such a method requires high resolution of the weak CT absorption band, that should be clearly distinguished from LE absorption band tails.

For the analysis, the experimental EQE spectrum is first measured at different temperatures showing clear features from the CT band absorption, followed by fitting using a simple Gaussian function at different temperatures. The extracted apparent E_{CT}(exp.) typically shows a significant downward trend as temperature decreases due to relaxation of excitons in the DOS. At low temperature ($T \rightarrow 0$ K), the line width is limited, which is a temperature-independent feature caused by the static distribution of CT states, *i.e.* static disorder. The Stokes shift is then no longer fixed at 2λ, which cannot be directly explained by Marcus theory. Burke *et al.*[74] proposed a physical model that regards the CT state as a Gaussian distribution rather than a single energy level, where the characteristic parameters of the CT state density distribution are the center energy of CT DOS (E_{CT}) and the standard deviation (σ_{CT}) (representing the degree of static disorder). When the Gaussian distribution is

convoluted with the dynamic broadening of the molecular vibrations, the resulting absorption spectrum (measured by EQE) can be described by the following expression:

$$\eta_{EQE}(E) \propto \frac{1}{E\sqrt{2\pi(\sigma_{CT}{}^2 + 2\lambda k_B T)}} \exp\left(\frac{-(E_{CT} + \lambda - E)^2}{2\sigma_{CT}{}^2 + 4\lambda k_B T}\right) \quad (17)$$

where E is the photon energy. This form separates the contribution of static disorder ($\sigma_{CT}{}^2$) and temperature-dependent dynamic disorder ($\sqrt{2\lambda k_B T}$) into total spectral broadening.

It is very important to measure the sub-bandgap region of CT absorption characteristics with a high signal-to-noise ratio. Then, the CT absorption features in the EQE spectrum are fitted using the standard Gaussian function at each temperature. The central energy position of the CT feature may be a small peak in the rapid rise phase of the EQE curve. At this time, the apparent experimental parameters, peak energy E_{CT}(exp.) and apparent recombination energy λ(exp.), at each temperature can be extracted:

$$E_{CT}(\text{exp.}) = E_{CT} - \frac{\sigma_{CT}{}^2}{2k_B T} \quad (18)$$

$$\lambda(\text{exp.}) = \lambda + \frac{\sigma_{CT}{}^2}{2k_B T} \quad (19)$$

By plotting the relationship between the extracted E_{CT}(exp.) and λ(exp.) and the reciprocal of temperature ($1/T$), the slopes can be used to extract the true E_{CT} and λ, respectively. However, one should be reminded that this method relies on the assumption of Gaussian type DOS, which might not be true in some material systems.[77] A more general type of DOS may be considered to deliver a better resolution of CT properties.[50]

5.1.2 Spectral deduction (EL–PL). In the second method, for systems with some but not complete spectral overlap between the LE and CT state emission, an attempt can be made to subtract the appropriately normalized PL spectrum from the EL spectrum to eliminate the LE contribution and leave the residual CT emission signal. As previously explored by Perdigón-Toro *et al.*, assuming that the total EL spectrum is a linear combination of the CT state emission and the LE state emission, the subtraction of the appropriately normalized PL spectrum from the EL spectrum reveals a broad low-energy residual feature, and the spectrum can theoretically be analyzed in isolation to determine the properties of the CT state.[42] However, such a method needs to be carried out with caution, specifically by normalizing the integral area or peak height of the two curves. Since the subtracted signals from EL–PL are often very weak, and may easily be impacted by the levels of injection in EL experiments.

5.2 Invisible CT states

The invisible CT state refers to the completely covered CT emission and absorption in standard EL and PL experiments. This has now become a common feature and issue in the state-of-the-art NFA based OPVs, making it difficult to acquire properties of CT states, *e.g.* its state energy and reorganization energies. Here we discuss two methods that have been explored in the literature that can be helpful for probing the invisible CT states.

5.2.1 Electro-absorption spectroscopy. The first method is electro-absorption spectroscopy (EAS), also known as Stark spectroscopy.[78–81] EAS is a method to measure the absorbance change (ΔA) caused by the electric field F_{app} by using the external electric field to disturb the molecular ground state and excited state energy levels (Stark effect). For a fixed and isotropic sample, the ΔA spectrum can be described by the Liptay equation[82,83] as a Taylor series expansion:

$$\Delta A = A^F(E) - A(E) = (k-1)A(E) + k\Delta E \times \frac{dA}{dE} + \frac{k\Delta E^2}{2} \times \frac{d^2A}{dE^2} \quad (20)$$

where $A^F(E)$ and $A(E)$ are the absorption spectra with (field-on) and without (field-off) applied field, respectively. The energy change ΔE includes contributions from the linear and quadratic Stark effects:

$$\Delta E = -\tfrac{1}{2}\Delta p F^2 + \Delta\mu F \quad (21)$$

where Δp and $\Delta\mu$ represent the change in polarizability and dipole moment. And considering the dielectric constant of the medium (ε) in non-polar environments, the effective electric field $F = (2\varepsilon + 1)F_{app}/3$.[84]

A Frenkel or local exciton transition refers to the process of electron transition to higher orbitals in the same molecule or chromophore. Its ground state and excited state are relatively non-polar, and the change in $\Delta\mu$ is usually small. Therefore, the EAS signal is mainly affected by the change in polarizability (Δp), and the spectral feature has a linear shape of the first derivative. On the other hand, the CT transition consists of spatially separated electron–hole pairs (D^-–A^+) with a very large electric dipole, and the variation of $\Delta\mu$ is usually larger. Therefore, a strong EAS signal dominated by the second-order derivative is generated, and the spectral feature is mainly in the form of a second derivative. This means that the shape of the EAS spectrum measured in the experiment is highly similar to the second derivative curve of the absorption peak in the CT state. The central energy of each Gaussian function used to fit the CT absorption band represents the energy of such CT manifold. The fitting formula is:

$$\Delta A \approx \frac{1}{2} C_L \Delta\mu^2 F^2 \frac{d^2A}{dE^2} \quad (22)$$

where the constant C_L is obtained through experiments, with a value of 1/3.

Based on the method described above, the experimental starting point is to obtain the absorption spectrum ($A(E)$) in the absence of an applied electric field. Based on this, a known electric field F_{app} is applied to measure the resulting spectral absorption change, namely the electrical absorption spectrum or Stark spectrum (ΔA). After obtaining these two sets of spectral data, the absorption band characteristic attributable to the CT transition must be identified in the $A(E)$ spectrum. To accurately analyze this characteristic and to avoid interference from

experimental noise in subsequent calculations, a series of Gaussian functions are typically used to reconstruct or fit the CT absorption band. This step not only provides a spectral line shape that can be accurately differentiated, but also reveals the energy distribution of the CT state attributable to the central energy of the Gaussian functions fitted to the CT absorption band. Finally, to verify the accuracy of such an energy distribution, the smoothed absorption spectrum obtained by Gaussian fitting is first- and second-order differentiated and used as basis functions to fit the experimentally measured ΔA spectrum. This is because the line shape of the electrical absorption signal of the CT state is primarily determined by the second-order derivative of the original absorption spectrum, from which the energy of the CT state can be extracted.

5.2.2 Advanced model fitting. The final method is to extract CT state properties using the previously developed MLJ model coupled with drift and diffusion equations (introduced in the previous section). This theoretical framework allows the modelling of the complete process from exciton generation to charge collection, and the properties of important states, *i.e.* LE, CT, and charge separated state (CS), are all considered. In a previous study by Müller *et al.*, using this model, they realized simultaneous fitting of current–voltage (*JV*) characteristics and PL, and extracted CT properties even when it's not visible in EQE, EL and PL.[85] The authors used $\Delta E_{\mathrm{LE-CT}}$, LE dissociation rate ($k_{\mathrm{LECT}}^{\mathrm{dis}}$), CT dissociation rate ($k_{\mathrm{CTCS}}^{\mathrm{dis}}$), and mobility ($\mu$) as fitting variables. The absolute PL intensity is used to determine $k_{\mathrm{LECT}}^{\mathrm{dis}}$, considering the competition between LE exciton dissociation and decay.[85] $k_{\mathrm{CTCS}}^{\mathrm{dis}}$ can be determined from the model by simultaneously fitting J_{sc} and FF. They found $k_{\mathrm{CTCS}}^{\mathrm{dis}}$ of 10^{10} s^{-1} for the high-offset blends and of 10^{7} s^{-1} for the low-offset blends, which are important reasons for low offset systems to deliver low charge generation yield. In addition, by linking the kinetic rate to free energy difference through the principle of detailed balance, the method can extract the energy of the charge separated state (E_{CS}) and the energetic barrier between CT and CS, *i.e.* $\Delta E_{\mathrm{CT,CS}}$. This method has the potential to be further explored to include more experimental data in the fitting procedure, to enhance the accuracy of extracted properties of the invisible CT state.

6 A general guide

Although classical Marcus theory has become a successful and routine tool for analyzing CT states, it requires extra caution when applied to modern high-performance NFA systems. Based on the several advanced methods introduced earlier, we provide the following guide to the probing and analysis of CT states, which is also summarized as a decision tree in Fig. 10.

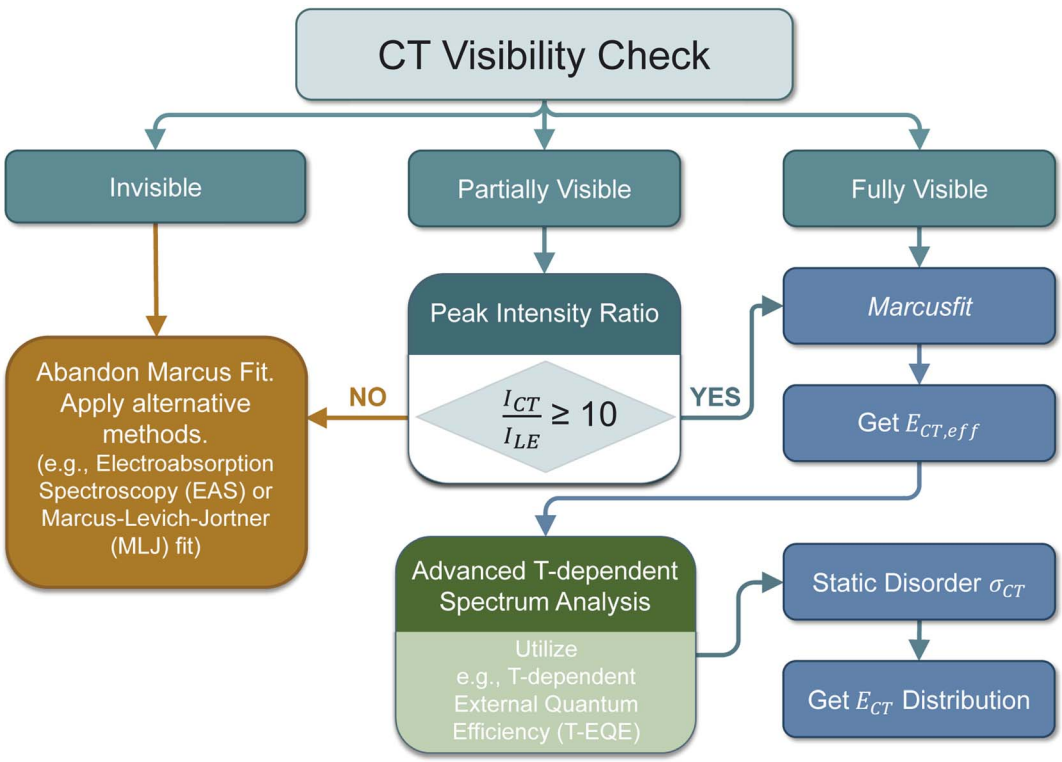

Fig. 10 Decision tree for Marcus fitting of $\mathrm{EQE_{PV}}$ and EL spectra. The flowchart outlines a systematic protocol based on the visibility of CT emission feature in EL experimental spectra. Starting with a "CT Visibility Check," the procedure branches into three pathways: (i) invisible. Marcus fitting is abandoned in favor of alternative methods such as electroabsorption spectroscopy (EAS) or Marcus–Levich–Jortner (MLJ) fitting; (ii) partially visible. The peak intensity ratio $I_{\mathrm{CT}}/I_{\mathrm{LE}}$ is evaluated; if ≥10, Marcus fitting proceeds to obtain effective CT energy ($E_{\mathrm{CT,eff}}$), followed by advanced temperature-dependent spectral analysis (*e.g.*, T-EQE) to extract static disorder (σ_{CT}) and the final E_{CT} distribution; otherwise, alternative methods are applied; (iii) fully visible. Marcus fitting is directly applied to derive $E_{\mathrm{CT,eff}}$, and then refined *via* temperature-dependent analysis to yield σ_{CT} and the final E_{CT} distribution.

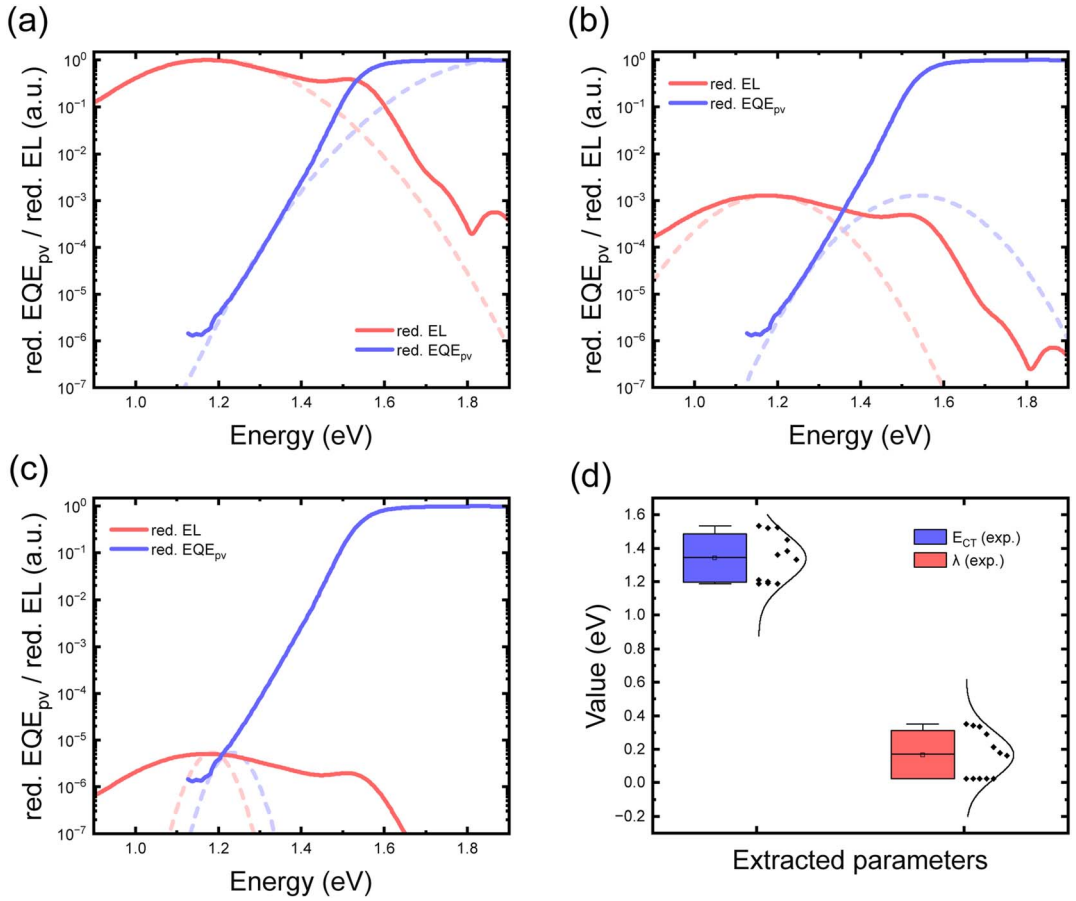

Fig. 11 Summary of the results for fitting EL and EQE spectra of PM7/IT4F blends[86] using the classical Marcus theory. (a–c) The fitting results for either the shoulder peak or the EQE tail are difficult to simultaneously fit spectral features such as peak intensity, linewidth, and the intersection of the EL and EQE curves. (d) Error statistics of results from multiple fittings using the classical Marcus fitting.

It is recommended that the first step of any analysis be to carefully examine the low-energy absorption and emission spectra of the device, typically EQE and EL spectra. If the CT features can be clearly seen in the EQE or EL spectra of a large offset system either partially or fully, classical Marcus fitting can be performed. The fitting program *Marcusfit* that we have made public on Github will be a very convenient tool.[73] *Marcusfit* is built specifically to streamline this process by jointly analyzing both spectra. It mathematically identifies the intersection point of the normalized EL and EQE curves to establish initial parameter estimates, and employs a fine-tuning algorithm to extract the CT energy and reorganization energy with high numerical stability. However, it is suggested that the obtained CT energy E_{CT}(exp.) be interpreted as an effective energy rather than an absolute and single value. This is because the value is affected by the inherent static energetic disorder, causing the experimentally observed emission peak to deviate from the DOS center. Therefore, it is recommended that E_{CT}(exp.) be used only as a reference energy. Additionally, the value λ(exp.) extracted from the classical Marcus fitting contains two physically different phenomena: dynamic and static disorder. If the extracted reorganization energy (λ_o) from a classical Marcus fit at room temperature is unusually large, static disorder could be significant. The practical strategy is to perform temperature-dependent s-EQE or PL tests. Dynamic disorder is thermally activated and temperature-dependent ($\sigma_d = (2\lambda_o k_B T)^{1/2}$), while static disorder is essentially temperature-independent. Hence, static disorder can be isolated from dynamic effects by measuring the spectra across a range of temperatures and plotting the apparent CT parameters against $1/T$.

However, in modern OPVs, LE states are often very emissive, and CT signals are easily buried under those of LE. Hence, the classical Marcus fitting method often fails to yield physically reliable results. When CT absorption is weak, the fitting process usually struggles to capture meaningful CT signals; hence the error would be large. Here, we take the EL and EQE spectra measured by Wu *et al.*[86] in PM7/IT4F blends as an example and perform classical Marcus fitting, as shown in Fig. 11. In this case, the small energy difference between the LE and CT states leads to significant overlap between LE and CT emission with the peak intensity ratio between CT and LE being less than 10, which should give large errors in reorganization energy and CT state energy following the guidance provided in Fig. 10. Indeed, the fitting parameters extracted from this type of data have significant uncertainties and poor convergence, making it difficult to distinguish the true CT contribution from experimental noise. Therefore, the obtained reorganization energy

and CT state energy values lack physical reliability and should be interpreted with caution.

When the CT signal is completely obscured by the absorption tail of local excitons, attempting to fit this region using the classical Marcus model is a common but crucial mistake, as the fitting will mainly focus on the LE tail rather than the CT state. Therefore the fitting result is physically meaningless. If the CT features cannot be clearly identified by comparing the absorption or emission of pristine materials and blends, it is recommended to abandon the classical Marcus fitting. It would be beneficial to consider other methods. For instance, EAS is a powerful technique because it is highly sensitive to changes in the dipole moment (the decisive feature of CT transitions) and can be identified even if the CT state is hidden in conventional absorption spectroscopy.[81] Another approach can also be helpful, that is to employ advanced model fitting based on the MLJ model framework concerning both spectral and device characteristics as explored by Müller *et al.*[85] Through model fitting multiple experiments, one can obtain the properties of invisible CT states, including but not limited to state energy, inner and outer reorganization energies, static disorder, phonon energies, and the transition rate constants between LE, CT and CS states.

7 Conclusions

In summary, the classical Marcus single-state theory in the high temperature limit has limitations in the analysis of CT states in modern high-performance NFA based OPVs. The bright local excitonic state emission signal often masks the weak charge transfer state characteristics, and the material itself has static disorder. Therefore, directly applying the classical Marcus model for fitting may result in values that do not have true significance. We discuss the cause of such issues in detail and provide guidelines to avoid significant errors while performing Marcus analysis of CT states. If CT absorption and emission are visible or partially visible, the extracted values *via* Marcus fitting should only be regarded as "effective energies" given that static disorder is present. Meanwhile, the reorganization energies obtained through Marcus fitting should be treated with caution. It's suggested to employ temperature dependent spectroscopy to better resolve the impact of dynamic and static disorder. If the characteristics of the charge transfer state cannot be clearly identified in the sub-bandgap regions of the absorption and emission spectra, the classical Marcus fitting should be abandoned and advanced techniques such as electro-absorption spectroscopy should be adopted instead. Advanced models that account for more practical features of CT states can also be useful and can help extract more information about the hidden CT states.

Author contributions

L. L. and J. Y. wrote the manuscript. L. L. conducted the model calculations and developed *Marcusfit*. S. L., W. L., and X. L. gave critical review of the manuscript. J. Y. supervised the work.

Conflicts of interest

The authors declare no competing interests.

Data availability

All the data supporting the current study are available in its supplementary information (SI) files or from the corresponding authors upon reasonable request. The code is available *via* GitHub: https://github.com/junyannj/Marcusfit. Supplementary information: detailed parameters used to generate electroluminescence (EL) and external quantum efficiency (EQE) data, the theoretical framework and algorithm of Marcusfit program, specific mathematical formulas for spectral analysis, as well as the comparative validation results. See DOI: https://doi.org/10.1039/d5el00216h.

Acknowledgements

J. Y. acknowledges funding support from the National Natural Science Foundation of China (No. 62574175 and No. 62404191), the Guangdong Basic and Applied Basic Research Foundation (No. 2023A1515111140 and No. 2024A1515012318), the Guangdong Provincial Program (No. 2023QN10C144), the Shenzhen Science and Technology Program (No. KQTD20240729102028011 and No. JCYJ20240813113553067), and the Guangdong Basic Research Center of Excellence for Aggregate Science.

References

1 N. S. Hush and J. R. Reimers, *Coord. Chem. Rev.*, 1998, **177**, 37–60.
2 M. Bixon and J. Jortner, in *Advances in Chemical Physics*, 1999, pp. 35–202.
3 N. Sutin, in *Advances in Chemical Physics*, 1999, pp. 7–33.
4 K. C. Weston, *Energy Conversion*, West Publishing Company, 1992.
5 P. Würfel, *Physics of Solar Cells: From Principles to New Concepts*, Wiley-VCH Verlag GmbH, Weinheim, 2005.
6 S. R. Wenham, *Applied Photovoltaics*, Earthscan, 2007.
7 J. Nelson, *The Physics of Solar Cells*, World Scientific Publishing Company, 2003.
8 R. A. Marcus, *Rev. Mod. Phys.*, 1993, **65**, 599–610.
9 R. A. Marcus, *Discuss. Faraday Soc.*, 1960, **29**, 21–31.
10 R. A. Marcus, *J. Chem. Phys.*, 1956, **24**, 966–978.
11 W. F. Libby, *J. Phys. Chem.*, 1952, **56**, 863–868.
12 R. A. Marcus, *Faraday Discuss. Chem. Soc.*, 1982, **74**, 7–15.
13 R. A. Marcus, *Annu. Rev. Phys. Chem.*, 1964, **15**, 155–196.
14 R. A. Marcus, *J. Phys. Chem.*, 1963, **67**, 853–857.
15 E. V. Anslyn and D. A. Dougherty, *Modern Physical Organic Chemistry*, University Science Books, 2006.
16 R. A. Marcus, *J. Phys. Chem.*, 1968, **72**, 891–899.
17 J. Stubbe, D. G. Nocera, C. S. Yee and M. C. Chang, *Chem. Rev.*, 2003, **103**, 2167–2201.
18 J. Franck and E. G. Dymond, *Trans. Faraday Soc.*, 1926, **21**, 536–542.

19 E. Condon, *Phys. Rev.*, 1926, **28**, 1182–1201.
20 J. R. Miller, L. Calcaterra and G. Closs, *J. Am. Chem. Soc.*, 1984, **106**, 3047–3049.
21 G. L. Closs and J. R. Miller, *Science*, 1988, **240**, 440–447.
22 J. Benduhn, K. Tvingstedt, F. Piersimoni, S. Ullbrich, Y. Fan, M. Tropiano, K. A. McGarry, O. Zeika, M. K. Riede, C. J. Douglas, S. Barlow, S. R. Marder, D. Neher, D. Spoltore and K. Vandewal, *Nat. Energy*, 2017, **2**, 17053.
23 E. Collado-Fregoso, S. N. Pugliese, M. Wojcik, J. Benduhn, E. Bar-Or, L. Perdigón Toro, U. Hörmann, D. Spoltore, K. Vandewal, J. M. Hodgkiss and D. Neher, *J. Am. Chem. Soc.*, 2019, **141**, 2329–2341.
24 P. F. Barbara, T. J. Meyer and M. A. Ratner, *J. Phys. Chem.*, 1996, **100**, 13148–13168.
25 G. Pourtois, D. Beljonne, J. Cornil, M. A. Ratner and J. L. Brédas, *J. Am. Chem. Soc.*, 2002, **124**, 4436–4447.
26 Y.-A. Duan, Y. Geng, H.-B. Li, J.-L. Jin, Y. Wu and Z.-M. Su, *J. Comput. Chem.*, 2013, **34**, 1611–1619.
27 L. Liu, P. Eisenbrandt, T. Roland, M. Polkehn, P.-O. Schwartz, K. Bruchlos, B. Omiecienski, S. Ludwigs, N. Leclerc, E. Zaborova, J. Léonard, S. Méry, I. Burghardt and S. Haacke, *Phys. Chem. Chem. Phys.*, 2016, **18**, 18536–18548.
28 M. List, T. Sarkar, P. Perkhun, J. Ackermann, C. Luo and U. Würfel, *Nat. Commun.*, 2018, **9**, 3631.
29 J. Wang, H. Yao, Y. Xu, L. Ma and J. Hou, *Mater. Chem. Front.*, 2021, **5**, 709–722.
30 K. Vandewal, K. Tvingstedt, A. Gadisa, O. Inganäs and J. V. Manca, *Phys. Rev. B: Condens. Matter Mater. Phys.*, 2010, **81**, 125204.
31 J. Benduhn, F. Piersimoni, G. Londi, A. Kirch, J. Widmer, C. Koerner, D. Beljonne, D. Neher, D. Spoltore and K. Vandewal, *Adv. Energy Mater.*, 2018, **8**, 1800451.
32 V. Coropceanu, X.-K. Chen, T. Wang, Z. Zheng and J.-L. Brédas, *Nat. Rev. Mater.*, 2019, **4**, 689–707.
33 A. A. Bakulin, S. D. Dimitrov, A. Rao, P. C. Y. Chow, C. B. Nielsen, B. C. Schroeder, I. McCulloch, H. J. Bakker, J. R. Durrant and R. H. Friend, *J. Phys. Chem. Lett.*, 2013, **4**, 209–215.
34 J. Hustings, R. Bonné, R. Cornelissen, F. Morini, R. Valcke, K. Vandewal and J. V. Manca, *Front. Photonics*, 2022, **3**, 1050189.
35 K. Vandewal, J. Benduhn and V. C. Nikolis, *Sustainable Energy Fuels*, 2018, **2**, 538–544.
36 Y. Jiang, S. Sun, R. Xu, F. Liu, X. Miao, G. Ran, K. Liu, Y. Yi, W. Zhang and X. Zhu, *Nat. Energy*, 2024, **9**, 975–986.
37 J. Fu, H. Li, H. Liu, P. Huang, H. Chen, P. W. K. Fong, T. A. Dela Peña, M. Li, X. Lu, P. Cheng, Z. Xiao, S. Lu and G. Li, *Nat. Energy*, 2025, **10**, 1251–1261.
38 H. Chen, Y. Huang, R. Zhang, H. Mou, J. Ding, J. Zhou, Z. Wang, H. Li, W. Chen, J. Zhu, Q. Cheng, H. Gu, X. Wu, T. Zhang, Y. Wang, H. Zhu, Z. Xie, F. Gao, Y. Li and Y. Li, *Nat. Mater.*, 2025, **24**, 444–453.
39 C. Li, J. Song, H. Lai, H. Zhang, R. Zhou, J. Xu, H. Huang, L. Liu, J. Gao, Y. Li, M. H. Jee, Z. Zheng, S. Liu, J. Yan, X.-K. Chen, Z. Tang, C. Zhang, H. Y. Woo, F. He, F. Gao, H. Yan and Y. Sun, *Nat. Mater.*, 2025, **24**, 433–443.
40 Y. Shi, Y. Chang, K. Lu, Z. Chen, J. Zhang, Y. Yan, D. Qiu, Y. Liu, M. A. Adil, W. Ma, X. Hao, L. Zhu and Z. Wei, *Nat. Commun.*, 2022, **13**, 3256.
41 P. Cheng, G. Li, X. Zhan and Y. Yang, *Nat. Photonics*, 2018, **12**, 131–142.
42 L. Perdigón-Toro, L. Q. Phuong, S. Zeiske, K. Vandewal, A. Armin, S. Shoaee and D. Neher, *ACS Energy Lett.*, 2021, **6**, 557–564.
43 N. A. Ran, S. Roland, J. A. Love, V. Savikhin, C. J. Takacs, Y. T. Fu, H. Li, V. Coropceanu, X. Liu, J. L. Brédas, G. C. Bazan, M. F. Toney, D. Neher and T. Q. Nguyen, *Nat. Commun.*, 2017, **8**, 79.
44 D. Qian, S. M. Pratik, Q. Liu, Y. Dong, R. Zhang, J. Yu, N. Gasparini, J. Wu, T. Zhang, V. Coropceanu, X. Guo, M. Zhang, J.-L. Bredas, F. Gao and J. R. Durrant, *Adv. Energy Mater.*, 2023, **13**, 2301026.
45 F. Gao and O. Inganäs, *Phys. Chem. Chem. Phys.*, 2014, **16**, 20291–20304.
46 S. Few, J. M. Frost and J. Nelson, *Phys. Chem. Chem. Phys.*, 2015, **17**, 2311–2325.
47 Y. Zhong, M. Causa', G. J. Moore, P. J. Krauspe, B. Xiao, F. Günther, J. Kublitski, R. Shivhare, J. Benduhn, E. Baror, S. Mukherjee, K. M. Yallum, J. Réhault, S. C. B. Mannsfeld, D. Neher, L. J. Richter, D. M. Delongchamp, F. Ortmann, K. Vandewal, E. Zhou and N. Banerji, *Nat. Commun.*, 2020, **11**, 833.
48 X.-K. Chen, V. Coropceanu and J.-L. Brédas, *Nat. Commun.*, 2018, **9**, 5295.
49 F. D. Eisner, M. Azzouzi, Z. Fei, X. Hou, T. D. Anthopoulos, T. J. S. Dennis, M. Heeney and J. Nelson, *J. Am. Chem. Soc.*, 2019, **141**, 6362–6374.
50 J. Yan, E. Rezasoltani, M. Azzouzi, F. Eisner and J. Nelson, *Nat. Commun.*, 2021, **12**, 3642.
51 C. Kaiser, O. J. Sandberg, N. Zarrabi, W. Li, P. Meredith and A. Armin, *Nat. Commun.*, 2021, **12**, 3988.
52 S.-U.-Z. Khan and B. P. Rand, *Phys. Rev. Appl.*, 2021, **16**, 044026.
53 S. M. Hosseini, S. Wilken, B. Sun, F. Huang, S. Y. Jeong, H. Y. Woo, V. Coropceanu and S. Shoaee, *Adv. Energy Mater.*, 2023, **13**, 8.
54 C. Göhler, M. Saladina, Y. Wang, D. Spoltore, J. Benduhn, K. Leo and C. Deibel, *Phys. Rev. Appl.*, 2021, **15**, 064009.
55 F.-J. Kahle, A. Rudnick, S. Wedler, R. Saxena, R. Ammenhäuser, U. Scherf, S. Bagnich, H. Bässler and A. Köhler, *Adv. Energy Mater.*, 2022, **12**, 2103063.
56 R. A. Marcus and N. Sutin, *Biochim. Biophys. Acta, Rev. Bioenerg.*, 1985, **811**, 265–322.
57 Y. Georgievskii, C.-P. Hsu and R. Marcus, *J. Chem. Phys.*, 1999, **110**, 5307–5317.
58 J. Jortner, *J. Chem. Phys.*, 1976, **64**, 4860–4867.
59 J. Nelson, J. J. Kwiatkowski, J. Kirkpatrick and J. M. Frost, *Acc. Chem. Res.*, 2009, **42**, 1768–1778.
60 A. Migliore and A. Nitzan, *ACS Nano*, 2011, **5**, 6669–6685.
61 Y. Zhao and W. Liang, *Chem. Soc. Rev.*, 2012, **41**, 1075–1087.
62 A. Köhler and H. Bässler, *Electronic Processes in Organic Semiconductors: an Introduction*, John Wiley & Sons, 2015.
63 E. Kennard, *Phys. Rev.*, 1918, **11**, 29.

64 P. Moroshkin, L. Weller, A. Saß, J. Klaers and M. Weitz, *Phys. Rev. Lett.*, 2014, **113**, 063002.
65 B. I. Stepanov, *Dokl. Akad. Nauk SSSR*, 1957, **112**(5), 839–841.
66 U. Rau, *Phys. Rev. B: Condens. Matter Mater. Phys.*, 2007, **76**, 085303.
67 W. Shockley, *Bell Syst. Tech. J.*, 1949, **28**, 435–489.
68 K. Vandewal, K. Tvingstedt and O. Inganäs, in *Semiconductors and Semimetals*, ed. U. Würfel, M. Thorwart and E. R. Weber, Elsevier, 2011, vol. 85, pp. 261–295.
69 K. Vandewal, A. Gadisa, W. D. Oosterbaan, S. Bertho, F. Banishoeib, I. Van Severen, L. Lutsen, T. J. Cleij, D. Vanderzande and J. V. Manca, *Adv. Funct. Mater.*, 2008, **18**, 2064–2070.
70 M. Azzouzi, J. Yan, T. Kirchartz, K. Liu, J. Wang, H. Wu and J. Nelson, *Phys. Rev. X*, 2018, **8**, 031055.
71 A. Classen, C. L. Chochos, L. Lüer, V. G. Gregoriou, J. Wortmann, A. Osvet, K. Forberich, I. McCulloch, T. Heumüller and C. J. Brabec, *Nat. Energy*, 2020, **5**, 711–719.
72 M. Azzouzi, N. P. Gallop, F. Eisner, J. Yan, X. Zheng, H. Cha, Q. He, Z. Fei, M. Heeney, A. A. Bakulin and J. Nelson, *Energy Environ. Sci.*, 2022, **15**, 1256–1270.
73 *Marcusfit*, 2025, https://github.com/junyannj/Marcusfit.
74 T. M. Burke, S. Sweetnam, K. Vandewal and M. D. McGehee, *Adv. Energy Mater.*, 2015, **5**, 1500123.
75 A. Troisi, *Chem. Soc. Rev.*, 2011, **40**, 2347–2358.
76 M. Bixon, J. Jortner and J. W. Verhoeven, *J. Am. Chem. Soc.*, 1994, **116**, 7349–7355.
77 M. Saladina, C. Wöpke, C. Göhler, I. Ramirez, O. Gerdes, C. Liu, N. Li, T. Heumüller, C. J. Brabec, K. Walzer, M. Pfeiffer and C. Deibel, *Phys. Rev. Lett.*, 2023, **130**, 236403.
78 D. de Sa Pereira, C. Menelaou, A. Danos, C. Marian and A. P. Monkman, *J. Phys. Chem. Lett.*, 2019, **10**, 3205–3211.
79 A. Devižis, J. De Jonghe-Risse, R. Hany, F. Nüesch, S. Jenatsch, V. Gulbinas and J.-E. Moser, *J. Am. Chem. Soc.*, 2015, **137**, 8192–8198.
80 S. Mahadevan, T. Liu, S. M. Pratik, Y. Li, H. Y. Ho, S. Ouyang, X. Lu, H.-L. Yip, P. C. Y. Chow, J.-L. Brédas, V. Coropceanu, S. K. So and S.-W. Tsang, *Nat. Commun.*, 2024, **15**, 2393.
81 P. Wan, X. Chen, Q. Liu, S. Mahadevan, M. Guo, J. Qiu, X. Sun, S.-W. Tsang, M. Zhang, Y. Li and S. Chen, *J. Phys. Chem. Lett.*, 2021, **12**, 10595–10602.
82 W. Liptay, in *Excited States*, Elsevier, 1974, vol. 1, pp. 129–229.
83 L. Sebastian, G. Weiser and H. Bässler, *Chem. Phys.*, 1981, **61**, 125–135.
84 C.-Q. Cao, W. Long and H. Cao, *Phys. Lett. A*, 1997, **232**, 15–24.
85 J. S. Müller, M. Comí, F. Eisner, M. Azzouzi, D. Herrera Ruiz, J. Yan, S. S. Attar, M. Al-Hashimi and J. Nelson, *ACS Energy Lett.*, 2023, **8**, 3387–3397.
86 H. Wu, H. Lu, Y. Li, X. Zhou, G. Zhou, H. Pan, H. Wu, X. Feng, F. Liu, K. Vandewal, W. Tress, Z. Ma, Z. Bo and Z. Tang, *Nat. Commun.*, 2024, **15**, 2693.